Electricity and Magnetism at the Cellular Level

9

This chapter describes a number of topics related to charged membranes and the movement of ions through them. Topics range from the basics of how the presence of impermeant ions alters the concentration ratios of permeant ions, to the movement of ions under the combined influence of an electric field and diffusion, and to simple models for gating in ion channels in cell membranes. It also discusses mechanisms for the detection of weak electric and magnetic fields and the possible effects of weak low-frequency electric and magnetic fields on cells.

Section 9.1 discusses Donnan equilibrium, in which the presence of an impermeant ion on one side of a membrane, along with other ions that can pass through, causes a potential difference to build up across the membrane. This potential difference exists even though the bulk solution on each side of the membrane is electrically neutral. Section 9.2 examines the Gouy–Chapman model for the charge buildup at each surface of the membrane that gives rise to this potential difference. This same model is extended in three dimensions to the cloud of counterions surrounding each ion in solution—the Debye–Hückel model of Sect. 9.3.

Since water molecules have a net dipole moment, they align themselves so as to nearly cancel the electric field of each ion. Very close to the ion, the electric field is so strong that even complete alignment is insufficient to cancel the ion's field. This saturation of the dielectric is described in Sect. 9.4.

Ions move in solution by diffusion if there is a concentration gradient and by drift if there is an applied electric field. The Nernst–Planck equation (Sect. 9.5) describes this motion. When several ion species are moving through a membrane, there can be zero total electric current, even though there is a flow of each species. A constant-field model for this situation leads to the Goldman equations of Sect. 9.6.

The next two sections discuss channels in active cell membranes. Section 9.7 describes a simple model for gating—the opening and closing of channels—as well as limitations to the conductance of each channel imposed by diffusion to the mouth of the channel. Section 9.8 introduces noise—the fluctuations in channel current that limit measurement accuracy but also can be used to determine properties of the channels.

Section 9.9 shows how channels can detect very small mechanical motions, as in the ear, and how certain fish can detect very small electric fields in sea water. Both of these processes are working near the limit of sensitivity set by random thermal motion.

Section 9.10 introduces an area of great interest and controversy: whether weak, low-frequency electric and magnetic fields can have any effect on cells. We discuss some of the physical aspects of the problem and conclude that such effects are highly unlikely.

There are many similarities between the models for biological physics presented in this chapter and the models used in plasma physics (Uehara et al. 2000).

9.1 Donnan Equilibrium

There is usually an electrical potential difference across the wall of a capillary. There is also a potential difference across the cell membrane (or plasma membrane or cytoplasmic membrane), and the concentration of certain ion species is different in the intracellular and extracellular fluid. In Chap. 3, we saw that if the potential difference across the membrane is $v' - v$, an ion of valence z is in equilibrium when $C'/C = e^{-ze(v'-v)/k_BT}$. For this concentration ratio, there is no current, even if the membrane is permeable to the species. This result is a special case of the Boltzmann factor, more familiar in physiology as the Nernst equation (Eq. 3.34):

$$v' - v = -\frac{k_BT}{ze} \ln\left(\frac{C'}{C}\right) = -\frac{RT}{zF} \ln\left(\frac{C'}{C}\right).$$

R. K. Hobbie, B. J. Roth, *Intermediate Physics for Medicine and Biology*,
DOI 10.1007/978-3-319-12682-1_9, © Springer International Publishing Switzerland 2015

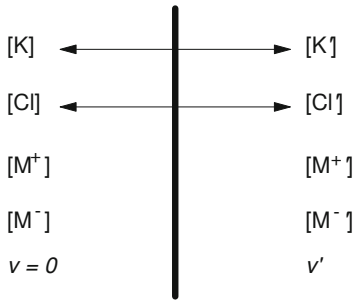

Fig. 9.1 Ion concentrations on either side of a membrane. Species that can pass through the membrane are indicated by double-headed arrows

It is often said—incorrectly—that the Nernst equation shows how the concentration of an ion species causes the potential difference across the membrane. We saw in Chap. 6 that the potential difference across the membrane is caused by layers of charge on each side of the membrane that create an electric field in the membrane. The solutions on each side of the membrane are electrically neutral except at the boundary with the membrane. (If there was an electric field in the solution, ions would move until the field was zero; then Gauss's law could be used to show that any volume contains zero charge.) We will learn in Sect. 9.2 the typical distance from the membrane occupied by the charged layer, and in Sect. 9.3, we will find the distance scale over which there are microscopic departures from neutrality in a bulk ionic solution.

The concentration differences do not *directly* cause the potential difference. However, if the concentration of an ion species on one side of the membrane is varied, the potential often changes in a manner that is approximated by the Nernst equation over a wide range of concentrations. We will now explore one mechanism by which this can happen. This is particularly important for the walls of capillaries, where charged proteins in the blood are too large to pass through the gaps between cells in the capillary walls, but it is also applicable to the cell membrane.

In Donnan equilibrium, the potential difference arises because one ion species cannot pass through the membrane at all. Consider the hypothetical case of Fig. 9.1. Permeant potassium ions exist on either side of the membrane in concentrations [K] and $[K']$. In this case, potassium is the only permeant cation; in a real situation, there might be several permeant ions. The membrane is also permeable to chloride ions, which exist in concentrations [Cl] and $[Cl']$. Chloride is the only permeant anion. In addition, there are large charged molecules $[M^+]$ and $[M^-]$ that cannot pass through the membrane. Their concentrations are $[M^+]$, $[M^{+\prime}]$, $[M^-]$, and $[M^{-\prime}]$. For simplicity, we assume they are monovalent. The potential on the left is 0; on the right, it is v'. Assume that the concentrations of the large molecules are fixed. The potassium concentration on the left side of the membrane will be assumed known, and we must solve for four variables: $[K']$, [Cl], $[Cl']$, and v'. Therefore, four equations are needed.

The first two equations state that the solutions on either side are electrically neutral:

$$[M^+] + [K] = [Cl] + [M^-], \tag{9.1}$$

$$[M^{+\prime}] + [K'] = [Cl'] + [M^{-\prime}]. \tag{9.2}$$

Equation 9.1 can be solved for [Cl]. It will be convenient to define $[M] = [M^+] - [M^-]$ and $[M'] = [M^{+\prime}] - [M^{-\prime}]$:

$$[Cl] = [K] + ([M^+] - [M^-]) = [K] + [M]. \tag{9.3}$$

Note that adding any amount of KCl to the solution on the left automatically satisfies this equation, since any increase in [K] is accompanied by the same increase in [Cl].

The other two equations state that the concentrations of potassium and chloride on the two sides of the membrane are related by a Boltzmann factor. Since the valence $z = +1$ for [K] and -1 for [Cl], we have

$$\frac{[K']}{[K]} = \frac{[Cl]}{[Cl']} = e^{-ev'/k_BT}. \tag{9.4}$$

The chloride concentration on the right is $[Cl'] = [Cl]\left([Cl']/[Cl]\right) = [Cl]\left([K]/[K']\right)$, so that from Eq. 9.2 $[K'] + [M'] = [Cl]\left([K]/[K']\right)$. This can be rewritten as a quadratic equation in $[K']$, since [K] and $[M']$ are known and [Cl] is calculated from Eq. 9.3:

$$[K']^2 + [M'][K'] - [K][Cl] = 0.$$

The solution is

$$[K'] = \frac{-[M'] + \sqrt{[M']^2 + 4[K][Cl]}}{2}. \tag{9.5}$$

(The negative square root is discarded because it would give a negative potassium concentration.) Once we have solved for $[K']$, $[Cl']$ and v' are determined from Eq. 9.4. Solutions for different values of [K] are shown in Table 9.1 and Figs. 9.2 and 9.3 for the conditions

$$[M^+] = 145\,\text{mmol}\,\text{l}^{-1}, \quad [M^{+\prime}] = 15\,\text{mmol}\,\text{l}^{-1},$$

$$[M^-] = 30\,\text{mmol}\,\text{l}^{-1}, \quad [M^{-\prime}] = 156\,\text{mmol}\,\text{l}^{-1},$$

$$[M] = 115\,\text{mmol}\,\text{l}^{-1}, \quad [M'] = -141\,\text{mmol}\,\text{l}^{-1}.$$

The temperature $T = 310$ K, for which $k_BT/e = 26.75$ mV.

Table 9.1 Variation of concentrations (mmol l^{-1}) and voltage (mV) as [K] is varied

[K]	[Cl]	[K′]	[Cl′]	[Cl]/[Cl′] = [K′]/[K]	v'
0.01	115.01	141.01	0.00816	14101	−255.57
0.10	115.10	141.08	0.08	1410.8	−193.99
0.20	115.20	141.16	0.16	705.8	−175.46
0.50	115.50	141.41	0.41	282.8	−151.00
1.00	116.00	141.82	0.82	141.8	−132.53
2.00	117.00	142.64	1.64	71.32	−114.15
5.00	120.00	145.13	4.13	29.03	−90.10
10.00	125.00	149.37	8.37	14.94	−72.33
20.00	135.00	158.08	17.08	7.904	−55.30
50.00	165.00	185.48	44.48	3.710	−35.07
100.00	215.00	233.20	92.20	2.332	−22.65
200.00	315.00	331.21	190.21	1.656	−13.49
500.00	615.00	629.49	488.49	1.259	−6.16

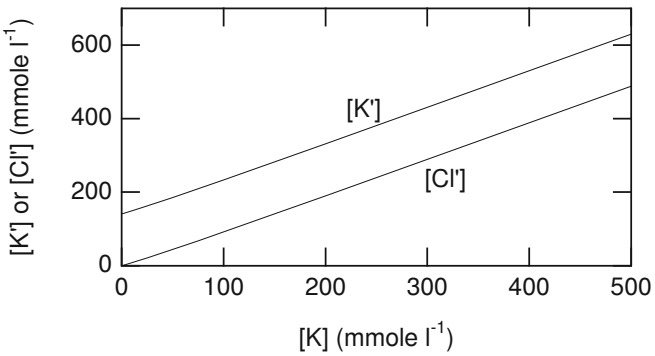

Fig. 9.2 Variation of [K′] and [Cl′] with [K] in the example of Donnan equilibrium

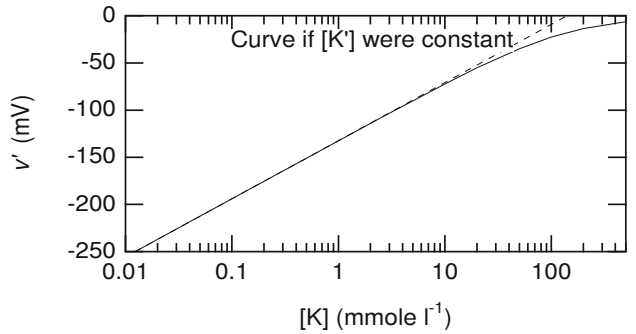

Fig. 9.3 Membrane potential v' vs. [K] for the example of Donnan equilibrium. For [K] $<$ 10 mM the curve is like the Nernst equation because [K′] has a nearly constant value of 141 mM. The dashed line shows the relationship if [K′] were constant

Several features of this solution are worth noting. First, changing [K] does change the potential, but the mechanism is indirect. The Boltzmann factor still applies; minuscule changes in concentration are sufficient to provide layers of charge on the membrane surface that generate a potential difference such that these concentrations are at equilibrium. Table 9.1 shows that [K] can vary by three orders of magnitude—from 0.01 to 10, and $[K']$ changes very little. Therefore, the curve of v' vs. ln [K] in Fig. 9.3 is nearly a straight line. The dashed line in Fig. 9.3 shows v' vs. ln [K] if $[K']$ is held constant. We could equally well have regarded [Cl] as the independent variable.

The impermeable ions enter the equation only as their net charge, $[M] = [M^+] - [M^-]$ and $[M'] = [M^{+\prime}] - [M^{-\prime}]$. As the concentrations [K] and [Cl] get larger, the impermeant ions become less important, the potential approaches zero, and the ratios $[K']$ / [K] and $[Cl']$ / [Cl] approach unity.

Donnan equilibrium may well explain the potential that exists across the capillary wall, which is impermeable to negatively charged proteins but is permeable to other ions. There is evidence that it does not adequately explain the potential across a cell membrane. For example, the membrane is known to be slightly permeable to sodium, although the sodium concentration is nowhere near what it would be if the sodium were in equilibrium.

9.2 Potential Change at an Interface: The Gouy–Chapman Model

In this section, we study one model for how ions are distributed at the interface in Donnan equilibrium. The model was used independently by Gouy and Chapman to study the interface between a metal electrode and an ionic solution. They investigated the potential changes along the x-axis perpendicular to a large plane electrode. The same model is used to study the charge distribution in a semiconductor. Biological applications are described by Mauro (1962). We show the features of the model by examining the transition region for the Donnan equilibrium example described in the preceding section.

An infinitely thin membrane at $x = 0$ is assumed to be permeable to potassium and chloride ions. Their concentrations are $K(x)$ and $Cl(x)$. An impermeant positive cation has concentration $M(x)$ for $x > 0$. For negative x, $M(x) = 0$. There are no impermeant anions. Far to the left, the potential is zero and the concentrations are [K] and [Cl]. Far to the right, they are v', $[K']$, $[Cl']$, and $[M']$.

The first step is to relate the charge distribution to the potential. If v and E change only in the x direction, then Gauss's law can be applied to a slab of cross-sectional area S between x and $x + dx$ as shown in Fig. 9.4. The net flux out through the surface at $x + dx$ is $E_x(x + dx)S$. The net outward flux at x is $-E_x(x)S$. There is no contribution to the flux through the other surfaces. The total ionic charge in the volume is $\rho_{\text{ext}}(x)Sdx$. We include the effect of water polarization by using the dielectric constant for water, which

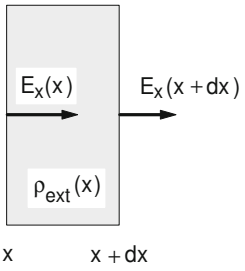

Fig. 9.4 Gauss's law is applied to the shaded volume to derive Poisson's equation in one dimension

is about $\kappa = 80$. Applying Gauss's law in the form of Eq. 6.21b, we obtain[1]

$$E_x(x+dx) - E_x(x) = \frac{4\pi\rho_{\text{ext}}(x)\,dx}{4\pi\epsilon_0\kappa},$$

$$\frac{dE_x}{dx} = \frac{4\pi\rho_{\text{ext}}(x)}{4\pi\epsilon_0\kappa}.$$

Finally, since $E_x = -\partial v/\partial x$, we have the one-dimensional Poisson equation,

$$\frac{d^2v}{dx^2} = -\frac{4\pi\rho_{\text{ext}}(x)}{4\pi\epsilon_0\kappa}. \tag{9.6}$$

This equation was derived in much the same way that the equation of continuity was combined with Fick's first law to derive Fick's second law (Sect. 4.8). The same procedure can be used in three dimensions to derive the general form of Poisson's equation:

$$\nabla^2 v = -\frac{4\pi\rho_{\text{ext}}(\mathbf{r})}{4\pi\epsilon_0\kappa}. \tag{9.7}$$

For the model being considered the ions are all univalent, so the ionic charge density at x is related to the concentrations by

$$\rho_{\text{ext}}(x) = e\,[K(x) + M(x) - Cl(x)]\,. \tag{9.8a}$$

More generally, for a series of ion species each with concentration C_i and valence z_i,

$$\rho_{\text{ext}}(\mathbf{r}) = e\sum_i z_i C_i(\mathbf{r}). \tag{9.8b}$$

[1] Throughout this section, we keep 4π in both numerator and denominator that could be canceled. We do this for two reasons. First, the quantity $1/4\pi\epsilon_0$ has a numerical value of about 9×10^9, which is easy to remember; second, for those who do not use SI units, the factor $1/4\pi\epsilon_0$ does not appear, but the other factor of 4π remains.

The next step is to assume that the concentrations of all ions are given by Boltzmann factors and are therefore related to the potential by

$$\begin{aligned} K(x) &= [\text{K}]\,e^{-ev(x)/k_BT} \quad \text{for all } x,\\ Cl(x) &= [\text{Cl}]\,e^{ev(x)/k_BT} \quad \text{for all } x,\\ M(x) &= \left[\text{M}'\right]e^{-e(v(x)-v')/k_BT}, \quad x>0. \end{aligned} \tag{9.9a}$$

(Remember that $M(x) = 0$ to the left of the origin.) An equivalent general expression is

$$\rho_{\text{ext}}(\mathbf{r}) = e\sum_i z_i\,[C_i]\exp\left[\frac{-z_i e v(\mathbf{r})}{k_BT}\right], \tag{9.9b}$$

where C_i is the concentration in the region where $v = 0$.

Combining Eqs. 9.7 and 9.9b gives the *Poisson–Boltzmann equation* for a dielectric:

$$\nabla^2 v = -\frac{4\pi e}{4\pi\epsilon_0\kappa}\sum_i z_i\,[C_i]\exp\left(\frac{-z_i e v(\mathbf{r})}{k_BT}\right). \tag{9.10}$$

For the specific problem at hand, the Poisson–Boltzmann equation takes the form

$$\frac{d^2v}{dx^2} = \frac{-4\pi e}{4\pi\epsilon_0\kappa}\left([\text{K}]\,e^{-ev(x)/k_BT} - [\text{Cl}]\,e^{ev(x)/k_BT}\right).$$

This applies for $x < 0$ only. While it is possible to solve this using numerical techniques (Mauro 1962), we will confine ourselves to the case in which $\xi = ev/k_BT \ll 1$, and we can make the approximation $e^{\xi} \approx 1+\xi$. (This is accurate to 0.5 % for $\xi = 0.1$, to 10 % for $\xi = 0.5$, and to 25 % for $\xi = 0.8$.) With this approximation

$$\begin{aligned} \rho_{\text{ext}} &= e\sum[C_i]\,z_i\left(1-\frac{z_i ev}{k_BT}\right) = \\ &e\sum[C_i]\,z_i - \frac{e^2}{k_BT}\sum[C_i]\,z_i^2 v. \end{aligned} \tag{9.11}$$

Far from the membrane the solution is electrically neutral, so the first term vanishes. We are left with the *linear Poisson–Boltzmann equation*:

$$\nabla^2 v(\mathbf{r}) = \frac{4\pi e^2\sum[C_i]\,z_i^2}{4\pi\epsilon_0\kappa\,k_BT}v(\mathbf{r}). \tag{9.12}$$

The coefficient of $v(\mathbf{r})$ on the right has the dimensions of $1/(\text{length})^2$. This length will also appear in other contexts. It is known as the *Debye length*, λ_D:

$$\frac{1}{\lambda_D^2} = \frac{4\pi e^2\sum[C_i]\,z_i^2}{4\pi\epsilon_0\kappa\,k_BT}. \tag{9.13}$$

The linearized Poisson–Boltzmann equation is

$$\nabla^2 v = \frac{v}{\lambda_D^2}. \tag{9.14}$$

For the one-dimensional problem and $x < 0$, it is

$$\frac{d^2v}{dx^2} = \frac{v}{\lambda_D^2}, \tag{9.15}$$

where

$$\frac{1}{\lambda_D^2} = \frac{4\pi e^2 ([\mathrm{K}] + [\mathrm{Cl}])}{4\pi\epsilon_0 \kappa k_B T}. \tag{9.16}$$

The methods of Appendix F can be applied to solve this equation.[2] The characteristic equation is $s^2 = 1/\lambda_D^2$, so the solution for $x < 0$ is $v(x) = Ae^{-x/\lambda_D} + Be^{x/\lambda_D}$. The potential is zero far to the left, so $A = 0$. Therefore, the solution is

$$v(x) = Be^{x/\lambda_D}, \quad x < 0. \tag{9.17}$$

It is most convenient to write the concentrations for $x > 0$ in terms of the concentrations far to the right. It is now necessary to include the impermeant ions.

$$\begin{aligned} K(x) &= [\mathrm{K}']\, e^{-e[v(x)-v']/k_B T}, \\ Cl(x) &= [\mathrm{Cl}']\, e^{e[v(x)-v']/k_B T}, \\ M(x) &= [\mathrm{M}']\, e^{-e[v(x)-v']/k_B T}. \end{aligned} \tag{9.18}$$

The linearized Poisson–Boltzmann equation for $x > 0$ is then

$$\begin{aligned} \frac{d^2v}{dx^2} = -\frac{4\pi e}{4\pi\epsilon_0\kappa}\Bigg(& [\mathrm{K}'] - \frac{[\mathrm{K}']\, ev(x)}{k_B T} + \frac{[\mathrm{K}']\, ev'}{k_B T} \\ & - [\mathrm{Cl}'] - \frac{[\mathrm{Cl}']\, ev(x)}{k_B T} + \frac{[\mathrm{Cl}']\, ev'}{k_B T} \\ & + [\mathrm{M}'] - \frac{[\mathrm{M}']\, ev(x)}{k_B T} + \frac{[\mathrm{M}']\, ev'}{k_B T} \Bigg). \end{aligned} \tag{9.19}$$

Neutrality requires that $[\mathrm{K}'] + [\mathrm{M}'] - [\mathrm{Cl}'] = 0$. With the definition

$$\frac{1}{\lambda_D'^2} = \frac{4\pi e^2([\mathrm{K}'] + [\mathrm{Cl}'] + [\mathrm{M}'])}{4\pi\epsilon_0\kappa k_B T}, \tag{9.20}$$

Eq. 9.19 can be written as

$$\frac{d^2v}{dx^2} - \frac{v(x)}{\lambda_D'^2} = -\frac{v'}{\lambda_D'^2}. \tag{9.21}$$

[2] We have seen this equation before in electrotonus when the membrane capacitance is fully charged (Sect. 6.12).

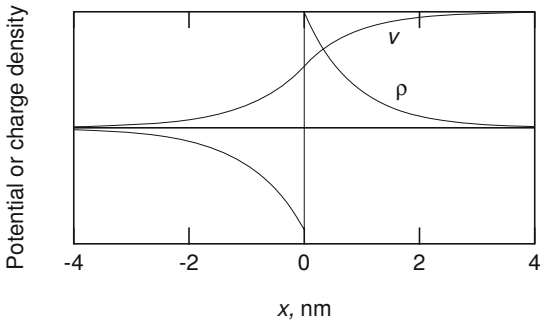

Fig. 9.5 The potential and charge density in the vicinity of the Donnan membrane. There is a layer of negative charge on the left of the membrane and of positive charge on the right. Each decays with the Debye length given by the ion concentrations far from the membrane

This is an inhomogeneous linear differential equation with constant coefficients. As pointed out in Appendix F, the most general solution is the sum of the solution to the homogeneous equation (i.e., with the right hand side equal to 0) and any solution of the inhomogeneous equation, with the constants adjusted to satisfy whatever boundary conditions exist. In this case, $v(x) = v'$ satisfies the inhomogeneous equation, so the most general solution is $v(x) = A'e^{-x/\lambda_D'} + B'e^{x/\lambda_D'} + v'$. Far to the right, $v = v'$ so $B' = 0$. Therefore, the solution we need is

$$v(x) = A'e^{-x/\lambda_D'} + v' \quad x > 0. \tag{9.22}$$

This solution for $x > 0$ must be combined with the solution for $x < 0$, Eq. 9.17. At $x = 0$ the potential must be continuous. Therefore $B = A' + v'$. Also at $x = 0$ the electric field, and therefore dv/dx, is continuous. (If dv/dx were not continuous, the second derivative and ρ_{ext} would be infinite.) This requirement gives the equation $B/\lambda_D = -A'/\lambda_D'$. Solving these two equations, we obtain

$$A' = \frac{-v'\lambda_D'}{\lambda_D' + \lambda_D}, \quad B = \frac{v'\lambda_D}{\lambda_D' + \lambda_D}. \tag{9.23}$$

Figures 9.5 and 9.6 show the potential, concentration, and charge density for the case $[\mathrm{K}] = 100$ and $[\mathrm{M}'] = 50$ mmol l^{-1}. The other parameters are given in Table 9.2. The value of $ev'/k_B T$ is 0.23.

Since the radii of ions are about 0.2 nm, the Debye length is several ionic diameters, and the continuous model we have used is reasonable.

The Poisson–Boltzmann equation is widely used to study charged molecules in solution (Honig and Nicholls 1995) and has implications for how proteins bind to DNA (Rohs et al. 2009). However, in small-scale systems such as ion channels, which have a size similar to or smaller than the Debye length, continuous models may not be entirely reliable (Moy et al. 2000).

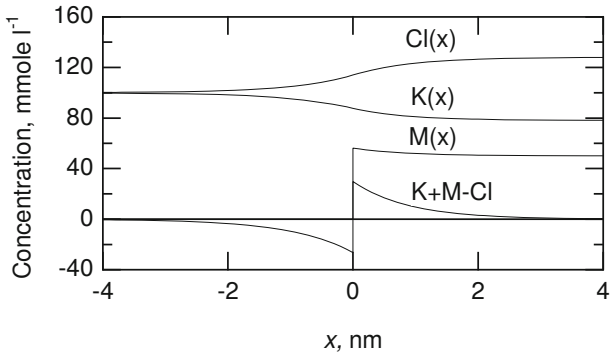

Fig. 9.6 Concentration profiles across the Donnan membrane. The concentration $K(x)+M(x)-Cl(x)$ is proportional to the charge density

Table 9.2 Parameters for the Donnan interface when [K] = 100, [M] = 0, and $[M'] = 50\,\text{mmol}\,l^{-1}$ at $T = 310$ K

[Cl]	$100\,\text{mmol}\,l^{-1}$
[K]	$100\,\text{mmol}\,l^{-1}$
[M]	$0\,\text{mmol}\,l^{-1}$
[K′]	$78.1\,\text{mmol}\,l^{-1}$
[Cl′]	$128.1\,\text{mmol}\,l^{-1}$
[M′]	$50\,\text{mmol}\,l^{-1}$
v'	6.617 mV
λ_D	0.991 nm
λ'_D	0.875 nm

The Gouy–Chapman model has been compared to detailed *molecular dynamics* simulations (in which every molecule is individually accounted for) for the case of salt water surrounding a lipid bilayer. The two computations are consistent as long as the adsorption of ions on the bilayer surface is accounted for (Yi et al. 2008).

9.3 Ions in Solution: The Debye–Hückel Model

In an ionic solution, ions of opposite charge attract one another. A model of this neutralization was developed by Debye and Hückel a few years after Gouy and Chapman developed the model in the previous section. The Debye–Hückel model singles out a particular ion and assumes that the average concentration of the counterions surrounding it is given by the Boltzmann factor. Screening by the counterions causes the potential to fall much more rapidly than $1/r$. One major difficulty with this assumption is that each counterion is also a central ion; therefore, the notion of a continuous cloud of counterions represents some sort of average.

We consider a situation in which the electric field, potential, and charge distribution are spherically symmetric. We could begin with Eq. 9.7 and look up the Laplacian operator in spherical coordinates. However, it is instructive to derive Poisson's equation for the spherically symmetric case. Consider two concentric spheres of radius r and radius $r + dr$. Apply Gauss's law to the volume contained between the two surfaces. If $\mathbf{E}$ is spherically symmetric, the flux through the inner sphere is $4\pi r^2 E(r)$. It points into the sphere and is therefore negative. The outward flux at $r + dr$ is

$$4\pi(r+dr)^2 E(r+dr) = 4\pi\left[r^2 + 2rdr + (dr)^2\right]\left[E(r) + \frac{dE}{dr}dr\right].$$

If we keep only terms of order dr or less, the outward flux through the outer sphere is

$$4\pi r^2 E(r) + 8\pi r E(r)dr + 4\pi r^2 \frac{dE}{dr}dr.$$

The net flux out of the volume is $8\pi r E(r)dr + 4\pi r^2(dE/dr)dr$. The total charge in the shell is $\rho_{\text{ext}}(r)$ times the volume of the shell, $4\pi r^2 dr$. Therefore, Gauss's law is

$$8\pi r E(r)dr + 4\pi r^2 \frac{dE}{dr}dr = \rho_{\text{ext}}(r)\frac{4\pi r^2}{\kappa\epsilon_0}dr$$

or

$$\frac{1}{r^2}\frac{d}{dr}\left(r^2 E(r)\right) = \frac{4\pi\rho_{\text{ext}}(r)}{4\pi\epsilon_0\kappa}. \tag{9.24}$$

Since $E(r) = -dv/dr$, the final equation for the potential is

$$\frac{1}{r^2}\frac{d}{dr}\left(r^2\frac{dv}{dr}\right) = -\frac{4\pi\rho_{\text{ext}}(r)}{4\pi\epsilon_0\kappa}. \tag{9.25}$$

The Poisson–Boltzmann equation in spherical coordinates, the analog of Eq. 9.10, is

$$\frac{1}{r^2}\frac{d}{dr}\left(r^2\frac{dv}{dr}\right) = -\frac{4\pi e}{4\pi\epsilon_0\kappa}\sum z_i\,[C_i]\exp\left(\frac{-z_i e v(r)}{k_B T}\right). \tag{9.26}$$

We again make a linear approximation to the Boltzmann factor to obtain the linear Poisson–Boltzmann equation for spherical symmetry:

$$\frac{1}{r^2}\frac{d}{dr}\left(r^2\frac{dv}{dr}\right) = \frac{1}{\lambda_D^2}v(r). \tag{9.27}$$

The Debye length λ_D is defined in Eq. 9.13. With the substitution $v(r) = u(r)/r$, the equation becomes

$$\frac{d^2u}{dr^2} = \frac{1}{\lambda_D^2}u(r), \tag{9.28}$$

which is the same as Eq. 9.15. Therefore, the solution is

$$v(r) = \frac{u(r)}{r} = \frac{Ae^{-r/\lambda_D} + Be^{r/\lambda_D}}{r}.$$

Requiring that $v(r)$ approaches 0 as $r \to \infty$ means that $B = 0$. For small r, the electric field (dv/dr) is that of an unshielded ion of charge ze. Therefore $A = ze/4\pi\epsilon_0\kappa$, and the final solution is

$$v(r) = \left(\frac{ze}{4\pi\epsilon_0\kappa}\right)\left(\frac{e^{-r/\lambda_D}}{r}\right). \tag{9.29}$$

Table 9.3 The Debye–Hückel potential for a monovalent ion in a solution of ions at the concentration given in Fig. 6.2 for the interior of an axon. Also shown are the unscreened potential, the parameter zev/k_BT, and the charge inside a sphere of radius r

r (nm)	$v(r)$ (mV)	$e/(4\pi\epsilon_0\kappa r)$ (mV)	ev/k_BT	$q(r)/e$
0.3	40.6	59.9	1.52	0.94
0.4	26.8	44.9	1.00	0.90
0.5	18.8	36.0	0.70	0.86
0.6	13.8	30.0	0.51	0.82
0.7	10.4	25.7	0.39	0.77
0.8	8.0	22.5	0.30	0.72
0.9	6.2	20.0	0.23	0.67
1.0	4.9	18.0	0.18	0.63
1.2	3.2	15.0	0.12	0.54
1.4	2.1	12.8	0.08	0.46
1.6	1.4	11.2	0.05	0.39
1.8	1.0	10.0	0.04	0.32
2.0	0.7	8.99	0.03	0.27
2.2	0.5	8.17	0.02	0.22
2.4	0.3	7.49	0.01	0.18
2.6	0.2	6.91	0.01	0.15
2.8	0.2	6.42	0.01	0.12
3.0	0.1	5.99	0.00	0.10

This is the potential of a point charge ze in a dielectric, modified by an exponential decay over the Debye length. From Eq. 9.13, one sees that the greater the concentration of counterions, the shorter the Debye length.

Table 9.3 shows the values of $v(r)$, $\xi = ev/k_BT$, and the potential from an unscreened point charge in water of dielectric constant 80, when the ion concentrations are those given in Fig. 6.3. A typical ion radius is about 0.2 nm. We will discover in the next section that the dielectric constant saturates for $r < 0.25$ nm. Therefore, values are given in Table 9.3 only for $r > 0.3$ nm. The table shows that the assumption $e^{\xi} \approx 1 + \xi$ is reasonable only for $r > 0.5$ nm. The Debye length is $\lambda_D = 0.77$ nm.

The charge density of the ion cloud can be obtained from Eqs. 9.25 and 9.29. The result is

$$\rho_{\text{ext}}(r) = \frac{-ze}{4\pi\lambda_D^2 r} e^{-r/\lambda_D}. \tag{9.30}$$

The total charge in the counterion cloud inside a sphere of radius a is

$$\int_0^a 4\pi r^2 \rho_{\text{ext}}(r)\, dr.$$

Adding to this a point charge ze at the origin gives the total charge due to both the ion and the counterion cloud inside radius a:

$$q(a) = ze\left(1 + \frac{a}{\lambda_D}\right) e^{-a/\lambda_D}. \tag{9.31}$$

This function approaches ze, the charge of the point ion, as $a \to 0$, and it approaches 0 as $a \to \infty$. Table 9.3 also shows the values of $q(a)/e$. Ninety percent of the counterion charge resides within 3 nm of the central ion. The charge on the central ion is half neutralized by charge in a sphere of radius 1.3 nm, about six ionic radii. Figure 9.7 shows schematically an ion of radius 0.2 nm. Since a monovalent ion will be neutralized by a single counterion, it is clear that the assumption of a continuous charge distribution equal to the average is a bit strained. The shaded circle of radius 0.25 nm represents the region in which the water molecules are completely polarized and the dielectric constant is less than 80; this is discussed in the next section. (We have ignored the fact that close to the central ion the linear approximation is not valid.)

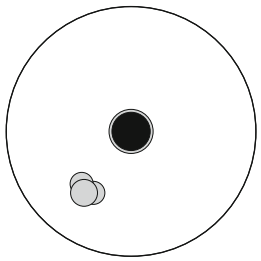

Fig. 9.7 Schematic picture of the regions surrounding an ion. The solid circle in the center represents the ion of radius 0.2 nm. The shaded circle shows the region in which the polarization of the water is saturated. The outer circle of radius 1.3 nm represents the region within which the cloud of counterions has neutralized half of the charge on the ion, which means that on the average a counterion will be in this region half of the time. This radius depends on the ion concentrations that are those for the interior of a squid axon. A scale drawing of a water molecule is also shown

When a highly charged molecule (for example, a strand of DNA) is surrounded by multivalent counterions, the counterions may interact so strongly that they are correlated with each other. Such effects are not included in the Debye–Hückel model. In some cases, these counterions cause charge inversion: so many correlated positive counterions form around a central negatively charged molecule that from a distance the molecule appears to have a net positive charge (Grosberg et al. 2002).

9.4 Saturation of the Dielectric

The electric field in vacuum at distance r from a point charge q is $E = q/(4\pi\epsilon_0 r^2)$. If the charge is in a dielectric, the field is reduced by a factor $1/\kappa$, except at very small distances, where the electric field is so strong that the polarization of the dielectric is saturated.

A molecule of water appears schematically as shown in Fig. 6.18. The radius of each hydrogen atom is about 0.12 nm; the radius of the oxygen is about 0.14 nm. Each hydrogen nucleus is 96.5 pm from the oxygen; the angle between them is 104 °. The hydrogen atoms share their electrons with the oxygen in such a way that each hydrogen atom has a net positive charge and the oxygen has a net negative charge. A pair of charges $\pm q$ separated by distance b has an *electric dipole moment* $\mathbf{p}_e$ of magnitude $p_e = qb$.

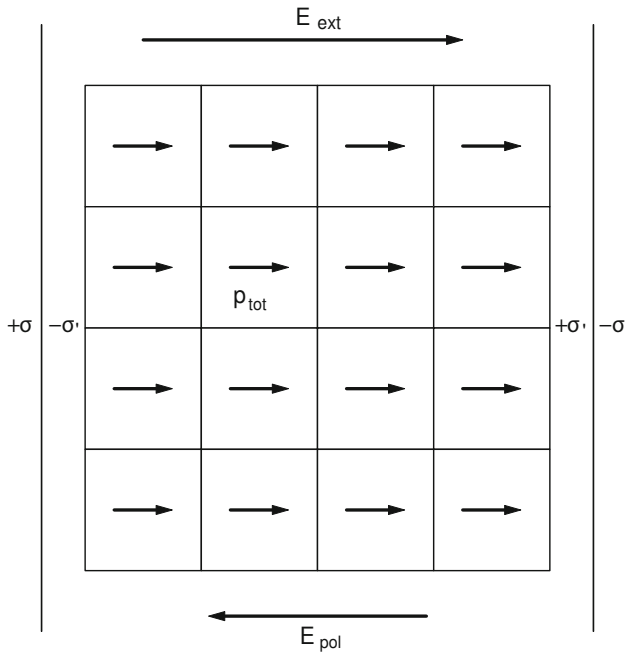

Fig. 9.8 A dielectric is placed in a parallel-plate capacitor that has charge density $\pm\sigma$ on each plate. A dipole moment of magnitude p_{tot} is induced in each volume element of the dielectric. The total effect is the same as a charge density $\pm\sigma'$ induced on the surfaces of the dielectric

The vector points from the negative to the positive charge. The magnitude of the dipole moment of a water molecule is 6.237×10^{-30} C m.

Each molecule of a dielectric in an applied electric field has an induced dipole moment that reduces the field. This dipole moment can be caused by a displacement of the electron cloud with respect to the nucleus, or it can represent (as for a polar molecule like water) an average molecular alignment against the tendency of thermal motion to orient the water molecules randomly.

The average induced dipole moment gives rise to the polarization field $\mathbf{E}_{\text{pol}}$ (Eqs. 6.19–6.20). To see the relationship, consider a small volume in the dielectric with N molecules per unit volume. Each molecule has an electric dipole moment $p_e = qb$. Far from this volume, the potential is primarily due to the dipole moment of each molecule. This can be shown by arguments like those in Sects. 7.3 and 7.4. The potential depends on the total dipole moment of the volume. The total number of dipoles in the volume is $NSdx$, so $p_{\text{tot}} = p_e NSdx$. This is equivalent to a charge $q' = p_e NS$ on the ends of the volume element, or a surface of charge density

$$\sigma'_q = \frac{q'}{S} = p_e N. \tag{9.32}$$

Now consider a parallel-plate capacitor as shown in Fig. 9.8. Imagine a series of small volume elements in the dielectric. The induced charges $\pm\sigma'_q$ on adjacent surfaces of each row of volume elements cancel except at the end of each row. The polarization field is therefore entirely due to the induced charge of surface density $\pm\sigma'_q$ at each end of the dielectric. The magnitude of the field is

$$E_{\text{pol}} = \frac{\sigma'_q}{\epsilon_0} = \frac{N p_e}{\epsilon_0}. \tag{9.33}$$

The quantity Np_e is the dipole moment per unit volume and is called the *polarization* P.

As the external electric field is increased, E_{pol}, which points in the opposite direction, also increases. This corresponds to the water molecules becoming more and more aligned. From the definition of susceptibility and the dielectric constant in Sect. 6.7, the magnitudes are related by

$$|E_{\text{pol}}| = \frac{\chi}{1+\chi}|E_{\text{ext}}| = \left(1 - \frac{1}{\kappa}\right)|E_{\text{ext}}|.$$

For a monovalent ion in water, $E_{\text{pol}} = (79/80)E_{\text{ext}} = (79/80)e/(4\pi\epsilon_0 r^2)$. When the dipoles are completely aligned, E_{pol} saturates at its maximum value, given by Eq. 9.33 with the molecular dipole moment substituted for p_e. The number of water molecules per unit volume is obtained from the fact that 1 mol has a mass of 18 g, occupies 1 cm^3 g^{-1}, and contains N_A molecules:

$$\begin{aligned} &E_{\text{pol}}(\text{max}) \\ &= \left[\frac{(N_A \text{ molecule mol}^{-1})(1 \text{ g cm}^{-3})(10^6 \text{ cm}^3 \text{ m}^{-3})}{(18 \text{ g mol}^{-1})\epsilon_0 \text{ C V}^{-1} \text{ m}^{-1}}\right] \\ &\times \left[6.237 \times 10^{-30} \text{ C m molecule}^{-1}\right] \\ &= 2.36 \times 10^{10} \text{ V m}^{-1}. \end{aligned}$$

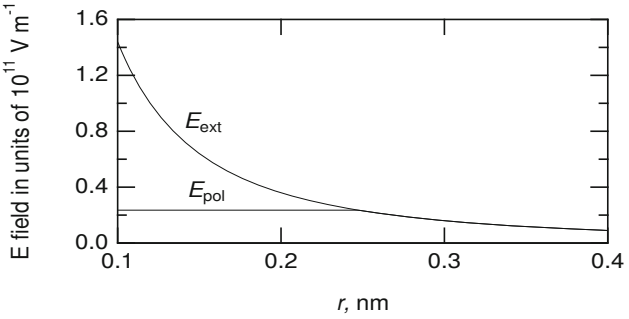

Fig. 9.9 The electric field around a monovalent point charge and the polarization electric field due to the water. The polarization field saturates for $r < 0.23$ nm

Figure 9.9 shows the fields E_{ext} and E_{pol} around a monovalent ion. As E_{pol} saturates, E_{tot} rises toward the value it would have without a dielectric. The dielectric constant falls

from 80 to 1 at about 0.23 nm. A more accurate model predicts similar behavior, but with a more gradual transition of the dielectric constant from 80 to 1.[3]

Close to an ion the potential is larger than $q/(4\pi\epsilon_0\kappa\, r)$. This changes the Born charging energy (Eq. 6.22), and the free energy change as an ion dissolves in a solvent (Bockris and Reddy 1970, Chap. 2). Also, close to an ion, the continuum approximation breaks down.

9.5 Ion Movement in Solution: The Nernst–Planck Equation

Solute particles can move by diffusion. They can also move if they have an average velocity V_{solute}. There are two ways they can acquire an average velocity. The first is if they are at rest on average with respect to a moving solution. This is called *solvent drag*. The second is for the solute particles to be dragged through the solution by an external force that acts on them, such as gravity or an electric force, balanced by the viscous force on the particles. In both cases, number per unit area per unit time crossing a plane is CV_{solute}. The solute particle fluence rate (particle current density) due to both diffusion and the solute velocity in the x direction is[4] (Sect. 4.12)

$$j_s = -D\frac{dC}{dx} + CV_{\text{solute}}. \tag{9.34}$$

Suppose that an external force $\mathbf{F} = ze\mathbf{E}$ acts on the solute particles in the x direction. They will be accelerated until the viscous drag on them is equal to the magnitude of F. But we saw in Chap. 4 that the viscous drag is $f = -\beta(V_{\text{solute}} - V_{\text{solvent}})$ where $V_{\text{solute}} - V_{\text{solvent}}$ is the relative velocity of the solute through the solvent. Coefficient β is related to the diffusion constant by $\beta = k_BT/D$. Therefore, the particles are no longer accelerated when

$$V_{\text{solute}} - V_{\text{solvent}} = zeE/\beta. \tag{9.35}$$

Equation 9.34 can be rewritten as

$$j_s = -D\frac{dC}{dx} + C\left[V_{\text{solvent}} + (V_{\text{solute}} - V_{\text{solvent}})\right].$$

Now V_{solvent} is the volume of solvent that flows per unit area per unit time and is just j_v. With this substitution and using Eq. 9.35, the particle current density is

$$j_s = -D\frac{dC}{dx} + Cj_v + CzeE\frac{D}{k_BT}. \tag{9.36}$$

[3] A more sophisticated model for the alignment of the electric dipoles in the electric field is analogous to that for magnetic moments in Sect. 8.3.

[4] We use x for the distance in the direction parallel to $\mathbf{E}$ because z is used for valence.

Table 9.4 Conductivities of ions at various concentrations at 25°C, calculated using Eq. 9.39. Diffusion constants for each ion are from Hille (2001, p. 317). Concentrations are typical of mammalian nerve and are from Hille (2001, p. 17). The conductivities of each species add, and $\rho = 1/\sigma$. Larger ions with very small diffusion constants make the solutions electrically neutral

	D (m^2s^{-1})	C (mmol l^{-1})	σ (S m^{-1})	ρ (Ω m)
Extracellular squid axon				
Na	1.33×10^{-9}	145	0.723	
K	1.96×10^{-9}	4	0.029	
Cl	2.03×10^{-9}	123	0.936	
			1.688	0.592
Intracellular squid axon				
Na	1.33×10^{-9}	12	0.060	
K	1.96×10^{-9}	155	1.139	
Cl	2.03×10^{-9}	4.2	0.032	
			1.231	0.812

The first term represents solute motion due to diffusion, the second represents solute dragged along with the bulk flow of the solution (solvent drag), and the third represents drift due to the applied electric field.

We will consider only the case in which there is no bulk flow of solution, so $j_v = 0$. The equation then reduces to the *Nernst–Planck equation*:

$$j_s = -D\frac{dC}{dx} + \frac{zeE}{k_BT}DC. \tag{9.37}$$

Diffusion is always toward the region of lower concentration, while for positive charge the V_{solute} term is in the direction of $\mathbf{E}$. For negative charges, it is in the opposite direction.

Consider the current density in bulk solution between planes at $x = 0$ where $v(x) = 0$ and $x = L$ where $v(x) = v$. If there is no concentration gradient and the potential changes uniformly, then $E = -dv/dx = -v/L$ points in the negative x direction, and the particle current density is $j_s = -zeDCv/k_BTL$. The electrical current density j is obtained by multiplying j_s by the charge on each particle, ze:

$$j = -\frac{z^2e^2DCS}{k_BTL}\frac{v}{S} = -\frac{G(C)}{S}v. \tag{9.38}$$

If $v(L) > v(0)$, the current is to the left and is negative. Recalling that $G = \sigma S/L = 1/R = S/\rho L$, we obtain the conductivity in the bulk solution

$$\sigma = \frac{1}{\rho} = \frac{z^2e^2DC}{k_BT}. \tag{9.39}$$

If several ion species carry current and can be assumed to move independently, then the total conductivity is the sum of the conductivities for each ion. Table 9.4 shows contributions to the conductivity for various species at typical concentrations.

This model is satisfactory for material such as the inside of an axon where the concentrations are constant and the material is electrically neutral, so that the ions themselves do not on average contribute to the electric field. We have assumed that the ions move independently, which will happen only if the electric field of other ions can be ignored.

We can model ions flowing from a region of one concentration to another (such as crossing the axon membrane) with the Nernst–Planck equation. Writing it for the electric current density and using the fact that $E(x) = -dv/dx$, we have

$$j = -zeD\frac{dC}{dx} - \frac{z^2e^2D}{k_BT}\frac{dv}{dx}C. \tag{9.40}$$

It is simpler to use the dimensionless variable $u(x) = zev(x)/k_BT$, which is the ratio of an ion's energy to thermal energy:

$$j = -zeD\left(\frac{dC}{dx} + C\frac{du}{dx}\right). \tag{9.41}$$

If we assume that dv/dx is constant throughout the region, $v(0) = 0$ and $v(L) = v$, then the gradient is $dv/dx = v/L$, and Equation 9.40 becomes

$$\frac{dC}{dx} - \frac{1}{\lambda}C = -\frac{j}{zeD}, \tag{9.42}$$

where the characteristic length for this model (*not* the Debye length) is

$$\lambda = -\frac{L}{u} = -\frac{k_BTL}{zev}. \tag{9.43}$$

Equation 9.42 is the same as Eq. 4.58, except for the denominator of the term involving j. Here the denominator is zeD because j is the electric current density instead of the particle current density. The solution analogous to Eq. 4.62 is

$$j = \frac{zeD}{\lambda}\frac{C_0e^{L/\lambda} - C_0'}{e^{L/\lambda} - 1} = \frac{zeD}{\lambda}\frac{C_0e^{-u} - C_0'}{e^{-u} - 1}, \tag{9.44}$$

where C_0 is the ion concentration at $x = 0$ and C_0' is the concentration at $x = L$.

The current vanishes if $C_0e^{L/\lambda} - C_0' = 0$, or $C_0'/C_0 = e^{L/\lambda} = e^{-zev/k_BT} = e^{-u}$. This is the Boltzmann factor.

Equation 9.44 can be written in terms of the original variables:

$$j = -\frac{z^2e^2Dv}{k_BTL}\frac{C_0e^{-zev/k_BT} - C_0'}{e^{-zev/k_BT} - 1} = -\frac{zeDu}{L}\frac{C_0e^{-u} - C_0'}{e^{-u} - 1}. \tag{9.45}$$

It is interesting to compare this to Eq. 9.38. Since G depends on concentration, it is useful to factor out C_0 and write

$$\begin{aligned} j &= -\frac{z^2e^2DC_0}{k_BTL}\frac{e^{-zev/k_BT} - C_0'/C_0}{e^{-zev/k_BT} - 1}v \\ &= -\frac{G(C_0)}{S}\frac{e^{-zev/k_BT} - C_0'/C_0}{e^{-zev/k_BT} - 1}v. \end{aligned} \tag{9.46}$$

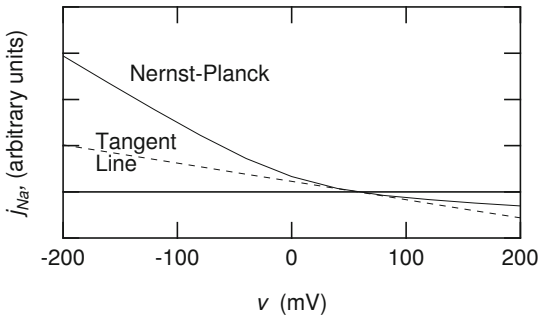

Fig. 9.10 Sodium current versus applied potential for the constant field Nernst–Planck model when the sodium concentration is 145 mM on the *left* and 15 mM on the *right*. The calculation was done using Eq. 9.45 for $T = 293$ K. The *tangent line* was calculated using Eq. 9.47. The nonlinearity or rectification occurs because of the different ion concentrations on each side

If $C_0 = C_0'$, we recover Eq. 9.38. Figure 9.10 shows the current density in A m^{-2} for a situation where $C_0 = 145$ and $C_0' = 15$ mmol l^{-1}. The diffusion constant for sodium from Table 9.4 has been used. As $C_0 > C_0'$, equilibrium occurs when $v = +57.3$ mV at 20°C.

Note the nonlinearity of the current–voltage relationship that arises because $C_0 \neq C_0'$. For very negative potentials, the flow is almost entirely from left to right and the current density approaches $G(C_0)v/S$ while for very positive potentials, the flow is from right to left and the current density approaches $G(C_0')v/S$. This asymmetry is fundamental. It occurs because there are different numbers of charge carriers on the left and right. When this behavior is seen in channels in cell membranes, they are often called *rectifier channels*. This same asymmetry in differences in the concentration of charge carriers is responsible for rectification in semiconductors.

Near the Nernst potential, the current density has the form $j = -(G/S)(v - v_{\text{Nernst}})$ if

$$\frac{G}{S} = \frac{G(C_0)(zev_{\text{Nernst}}/k_BT)}{S\left(e^{zev_{\text{Nernst}}/k_BT} - 1\right)}. \tag{9.47}$$

This equation was used to derive the tangent line shown in Fig. 9.10.

The constant-field model is an oversimplification. The field can be distorted by fixed charges near the channel through which the ions are flowing. Moreover, the model is internally inconsistent. There are electric fields generated by the flowing ions, which become important at high concentrations. The fact that $j = 0$ when the potential is equal to the Nernst potential is fundamental and holds for any ion or model for conduction. It can be derived in the general case from Eq. 9.42 (Problem 15). A self-consistent analytic solution for the case of a single ion species has been known for

50 years. The solution has been extended by many workers and has been generalized by Leuchtag and Swihart (1977) to the case in which all the ions have the same charge.

9.6 Zero Total Current in a Constant-Field Membrane: The Goldman Equations

The Nernst–Planck equation can be used to calculate the current due to movement of ions through a membrane in which there is a constant electric field. We assume a constant field because it leads to an analytic solution and because we have no knowledge of internal structure or the behavior of counterions which could change the field. The resulting equations are called the *Goldman* or the *Goldman–Hodgkin–Katz* (GHK) equations.

The GHK equations can be derived by assuming either a homogeneous membrane, in which case the Nernst–Planck equation is simply applied to each species, or cylindrical pores of constant cross section. Since we know that the pores do not have a constant electric field (Sect. 9.7) and it is quite unlikely that they have constant cross section, the GHK equations are an approximation. Nevertheless, they have been used widely in the study of excitable membranes.

We will show the derivation for a cylindrical pore that has a constant circular cross section. We use cylindrical coordinates (r, ϕ, x), where x is the axis of the cylinder. (Again, z denotes the valence of the ions.) Let the outside of the membrane be at $x = 0$ and the inside at $x = L$, where the potential is v and $u = zev/k_BT$. The arguments of Sect. 5.9 about the r and x dependence can be applied to Eq. 9.41. The analog of Eq. 5.37 is

$$j(r) = -zeD(r, a, R_p)\left(\frac{\partial C(r,x)}{\partial x} + \frac{u}{L}C(r,x)\right). \quad (9.48)$$

Again the concentration can be written as $C(r,x) = C(x)\Gamma(r)$. Equation 9.48 becomes

$$j(r) = -ze\Gamma(r)D(r, a, R_p)\left(\frac{\partial C(x)}{\partial x} + \frac{u}{L}C(x)\right). \quad (9.49)$$

This can be multiplied by $2\pi r\,dr$ and integrated over the pore area. There are two integrals to consider. The first defines the average current density for a particular species:

$$\int_0^{R_p} j(r)2\pi r\,dr = \pi R_p^2\,\bar{j}. \quad (9.50)$$

The second defines an effective diffusion constant:

$$\int_0^{R_p} \Gamma(r)D(r, a, R_p)2\pi r\,dr = \pi R_p^2 D_{\text{eff}}. \quad (9.51)$$

The integrated current density equation is

$$\bar{j} = -zeD_{\text{eff}}\left(\frac{dC(x)}{dx} + \frac{u}{L}C(x)\right). \quad (9.52)$$

Consideration of the r dependence in the pore has given an equation exactly like Eq. 9.41, but with D_{eff} instead of D. Equations 9.42 and 9.43 are still valid. The form of λ is unchanged: $\lambda = -k_BTL/zev$. Conversion from a single pore to unit area of the membrane requires multiplying $\bar{j}$ by $n\pi R_p^2$. As in Eq. 5.49 we define $\omega_s RT = n\pi R_p^2 D_{\text{eff}}/L$ and call the concentration outside C_1 and the concentration inside C_2. The electric current density per unit area of membrane is

$$\begin{aligned} J' &= \frac{z^2e^2\omega_s RTv}{k_BT}\frac{C_1e^{-zev/k_BT} - C_2}{1 - e^{-zev/k_BT}} \\ &= z^2e^2v\omega_s N_A\frac{C_1e^{-zev/k_BT} - C_2}{1 - e^{-zev/k_BT}}. \end{aligned} \quad (9.53)$$

Suppose that three species can pass through the membrane: sodium, potassium, and chloride. Equation 9.53 can be applied separately to each species to obtain the *GHK current equation* for each ion species:

$$J'_{\text{Na}} = e^2v\omega_{\text{Na}}N_A\frac{[\text{Na}_1]\,e^{-ev/k_BT} - [\text{Na}_2]}{1 - e^{-ev/k_BT}}, \quad (9.54a)$$

$$J'_{\text{K}} = e^2v\omega_{\text{K}}N_A\frac{[\text{K}_1]\,e^{-ev/k_BT} - [\text{K}_2]}{1 - e^{-ev/k_BT}}, \quad (9.54b)$$

$$J'_{\text{Cl}} = e^2v\omega_{\text{Cl}}N_A\frac{[\text{Cl}_1]\,e^{+ev/k_BT} - [\text{Cl}_2]}{1 - e^{+ev/k_BT}}. \quad (9.54c)$$

The *reversal potential*, v_{rev}, is the potential for which the total membrane current or fluence rate, that is the sum of the three fluence rates, is zero. The amount of charge within the cell does not change with time, but the concentration of each species within the cell changes with time. This less stringent requirement becomes $J'_{\text{Na}} + J'_{\text{K}} + J'_{\text{Cl}} = 0$. Adding Eqs. 9.54 together and factoring out $N_Ae^2v/(1 - e^{-ev/k_BT})$ gives

$$\begin{aligned} &(\omega_{\text{Na}}[\text{Na}_1] + \omega_{\text{K}}[\text{K}_1] + \omega_{\text{Cl}}[\text{Cl}_2])\,e^{-ev/k_BT} \\ &= \omega_{\text{Na}}[\text{Na}_2] + \omega_{\text{K}}[\text{K}_2] + \omega_{\text{Cl}}[\text{Cl}_1], \end{aligned}$$

or the *GHK voltage equation*

$$v_{\text{rev}} = \frac{k_BT}{e}\ln\left(\frac{\omega_{\text{Na}}[\text{Na}_1] + \omega_{\text{K}}[\text{K}_1] + \omega_{\text{Cl}}[\text{Cl}_2]}{\omega_{\text{Na}}[\text{Na}_2] + \omega_{\text{K}}[\text{K}_2] + \omega_{\text{Cl}}[\text{Cl}_1]}\right). \quad (9.55)$$

As an example of the use of the GHK voltage equation, consider how the reversal potential depends on the concentration of some external ion. We will use the concentrations of Fig. 6.2, except for the ion whose concentration is being changed. The particle concentrations are in mmol l^{-1} (any units can be used since ratios are taken):

$$[\text{Na}_1] = 145, \qquad [\text{Na}_2] = 15,$$

$$[\text{K}_1] = 5, \qquad [\text{K}_2] = 150,$$

$$[\text{Cl}_1] = [\text{Na}_1] + [\text{K}_1] - 25, \qquad [\text{Cl}_2] = [\text{Na}_2] + [\text{K}_2] - 156.$$

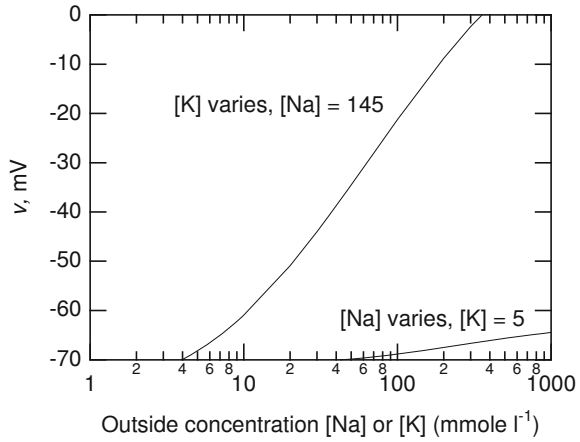

Fig. 9.11 The potential difference across a cell membrane as a function of changes in the exterior concentration of KCl or NaCl, calculated using the Goldman equation

The permeabilities are not known. However, only the ratio to ω_K matters. If we take the ratio $\omega_K : \omega_{Na} : \omega_{Cl}$ to be $1.0 : 0.04 : 0.45$ and use $T = 300$ K, then Eq. 9.55 is (in mV)

$$v = 25.88 \ln\left(\frac{[K_1] + 0.04\,[Na_1] + 0.45([Na_2] + [K_2] - 156)}{[K_2] + 0.04\,[Na_2] + 0.45([Na_1] + [K_1] - 25)}\right).$$

This has been plotted in Fig. 9.11 for variations of $[K_1]$ and $[Na_1]$. In each case, Cl ions are also added to the external solution in an equal amount. There is a region of potassium concentration over which the behavior is nearly exponential, and one could be misled into thinking that the potential–concentration relation was given either by the Nernst equation alone or by Donnan equilibrium. The potential change with sodium concentration is much less because of the low permeability of the membrane to sodium.

The assumption that the total current through the membrane is zero guarantees that there will be no charge buildup inside the cell; however, the individual currents are not zero, so there may be concentration changes with time. We will next investigate the magnitude of this effect. Equation 9.53 can be converted to particle flux instead of charge flux by dividing by ze. The result for ion s is

$$J_s = zev\omega_s \frac{C_1 e^{-zev/k_BT} - C_2}{1 - e^{-zev/k_BT}}.$$

The concentrations are converted from mmol l^{-1} to particles m^{-3} by multiplying by Avogadro's number. (The factors of 10^3 in the conversion happen to cancel out.) Consider the previous example at $T = 300$ K, $[K_1] = 5$, $[Na_1] = 145$, and $v = -68.17$ mV. The exponential factor for the positive ions is $e^{-ev/k_BT} = 13.929$, while for the chloride ion it is the reciprocal, 0.0718. If we write $\omega_{Na} = 0.04\omega_K$ and $\omega_{Cl} = 0.45\omega_K$, then the fluxes for the three ions are

$$J_K = +(6.55 \times 10^3)\omega_K(6.215),$$
$$J_{Na} = -(6.55 \times 10^3)\omega_K(6.202),$$
$$J_{Cl} = -(6.55 \times 10^3)\omega_K(0.013),$$

and the total current is zero.

Although the GHK equations are widely used because of their simplicity, some cautions are in order. Their derivation assumed independence of the moving ions. We know that this is an oversimplification for several reasons. Experiments show that the currents saturate for high concentrations. The distortion of the electric field by other ions was ignored. The permeability (diffusion constant) was assumed to be constant. The pore was assumed to have a constant cross-section and constant electric field. A somewhat less restrictive model for the reversal potential (the potential at which the current density becomes zero and changes sign) can be derived for a pair of ions with the same valence if we assume that any variations in $D(x)$ for the two ions are similar (Problem 20). With that assumption, the reversal potential is

$$v_{rev} = \frac{k_BT}{ze} \ln\left(\frac{\omega_a C_{a1} + \omega_b C_{b1}}{\omega_a C_{a2} + \omega_b C_{b2}}\right). \tag{9.56}$$

When ions have different valences, the GHK equation becomes more complicated. Lewis (1979) has derived an analogous equation for transport of sodium, potassium, and calcium.

9.7 Membrane Channels

In Chap. 6, we described some of the properties of the sodium and potassium channels in a squid axon. There are many other kinds of channels. Variations exist not only from one organism to another, but in different kinds of cells in the same organism. The classic monograph on ion channels is the book by Hille (2001). Genetic mutations of these channel proteins can cause diseases known as *channelopathies* (Ashcroft 2012).

There are several different kinds of potassium channels. Most open after depolarization; a few open after hyperpolarization. Potassium channels in axons (like the ones we encountered in Chap. 6) are called *delayed rectifiers* because of their delay in opening after a voltage step.

The properties of sodium channels are more uniform from one cell type to another.

Calcium channels pass much smaller currents than sodium or potassium channels because calcium concentrations are much smaller; the calcium current density is usually about one tenth the current density for sodium or

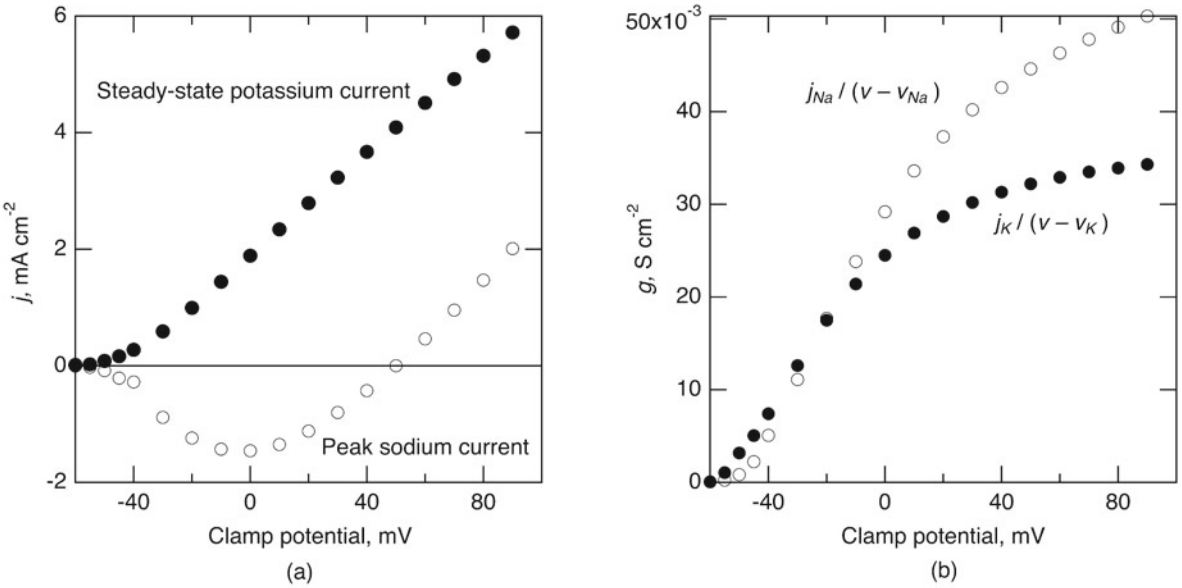

Fig. 9.12 Steady-state potassium current and peak sodium current for a squid axon subject to a voltage clamp vs. the transmembrane potential during the clamp. These are not real data, but were generated using the Hodgkin–Huxley model. **a** Current density. **b** Current density divided by the difference between the potential and the Nernst potential, to give the conductance per unit area. (see Eq. 6.61)

potassium. Calcium channels typically activate with depolarization. Since the concentration of calcium inside cells is usually very small, the interior calcium concentration can increase 20-fold in response to depolarization. This increase in concentration can initiate a chemical reaction, for example, to cause contraction of a muscle cell.

Chloride channels often have a large conductivity. The chloride concentration ratio in some muscle cells is such that the resting potential is close to the chloride Nernst potential. As a result, small changes in the potential cause relatively large chloride currents, which tend to stabilize the resting potential.

The earliest voltage-clamp measurements were difficult to sort out. Hodgkin and Huxley changed the concentration of extracellular sodium, substituting impermeant choline ions, to determine what part of the current was due to sodium and what was due to potassium. Figure 9.12(a) shows typical currents.

In the mid-1960s, various drugs were found that at very small concentrations selectively block conduction of a particular ion species. We now know that these drugs bind to the channels that conduct the ions. An example is *tetrodotoxin* (TTX), which binds to sodium channels and blocks them, making it a deadly poison.

The next big advance was *patch-clamp recording* (Neher and Sakmann 1976). Micropipettes were sealed against a cell membrane that had been cleaned of connective tissue by treatment with enzymes. A very-high-resistance seal

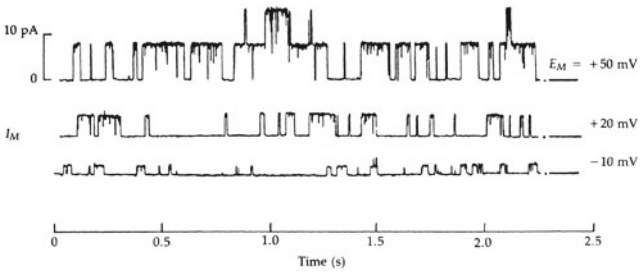

Fig. 9.13 Opening of single K(Ca) channels. (From Pallotta et al. (1981). Reprinted with permission from Nature (London))

resulted [(2–3)×10^7 Ω] that allowed one to see the opening and closing of individual channels. For this work, Erwin Neher and Bert Sakmann received the Nobel Prize in Physiology or Medicine in 1991. Around 1980, Neher's group found a way to make even higher resistance (10^{10}–10^{11} Ω) seals that reduced the noise even further and allowed patches of membrane to be torn from the cell while adhering to the pipette (Hamill et al. 1981). The relationship of noise to resistance will be discussed below.

The patch-clamp studies revealed that the pores open and close randomly, as shown in Fig. 9.13. Thus, the Hodgkin–Huxley model describes the average behavior of many pores, not the kinetics of single pores. Note how the current through

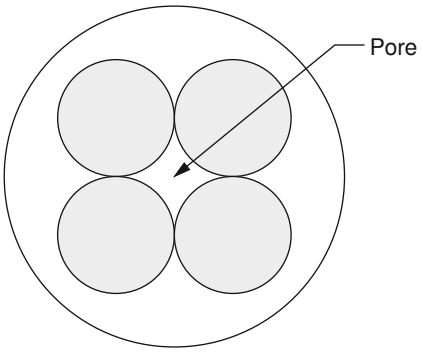

Fig. 9.14 The structure of a *Shaker* potassium channel. There are four subunits that traverse the membrane and create a pore at their center

an open pore changes as a function of the applied potential. A single open pore can pass at least 1 pA of current or 6×10^6 monovalent ions per second. Most can pass much more. While no perfectly selective channel is known, most channels are quite selective; for example, some potassium channels show a 100:1 preference for potassium over sodium.

Gene splicing combined with patch-clamp recording provided a wealth of information. Regions of the DNA responsible for synthesizing the membrane channel have been identified. One example that has been extensively studied is a potassium channel from the fruit fly, *Drosophila melanogaster*. The *Shaker* fruit fly mutant shakes its legs under anesthesia. It was possible to identify exactly the portion of the fly's DNA responsible for the mutation. When *Shaker* DNA was placed in other cells that do not normally have potassium channels, they immediately made functioning channels.

The current view is that the *Shaker* potassium channel consists of four subunits that span the membrane. The pore presumably runs along the four fold-symmetry axis, as shown in end view in Fig. 9.14. Sodium and calcium channels are very similar. Voltage-gated channels are reviewed by Sigworth (1993) and by Keynes (1994).

Roderick MacKinnon and his colleagues determined the three-dimensional structure of a potassium channel using X-ray diffraction (Doyle et al. 1998; Jiang et al. 2003). MacKinnon received the 2003 Nobel Prize in Chemistry for his work on the potassium channel.

The channel protein contains four identical subunits, arranged with four-fold symmetry around a central pore (Fig. 9.14). Each subunit has two alpha helices that cross the membrane and an inner pore region. One of the remarkable features of this channel is that potassium ions are 10,000 times more likely to pass through than sodium ions. Yet, potassium and sodium have similar chemistry (they are in the same column of the periodic table), and their ions are identical except for size (0.133 nm radius for potassium, 0.095 nm for sodium). The channel structure suggests that a narrow, 1.2 nm long region of the pore is responsible for selectivity. As the ion enters this region, there is not enough room for the polar water molecules that normally surround it and shield its charge. Instead, carbonyl oxygen atoms on the channel protein come in close contact with the potassium ion and provide the shielding. The size of the pore is such that potassium ions fit snugly with the surrounding carbonyl oxygen atoms, but sodium does not fit as well.

X-ray diffraction studies have also clarified the mechanism of voltage dependence in potassium channels. The pore is surrounded by the charged structures on the channel's perimeter that sense the transmembrane voltage. These structures act somewhat like levers, opening and closing the pore in response to the voltage. The movement of these structures is responsible for gating currents in these channels.

The structure of the sodium channel has recently been determined (Payandeh et al. 2011).

Let us now explore some of the physics of ion channels. Combining the macroscopic current density with the current in a single channel shows that there are not many channels per unit area of the membrane (see Problems 21 and 22). It is illuminating to consider what effect currents of this magnitude and duration have on the transmembrane potential. The capacitance per unit area of biological membranes is about 0.01 F m^{-2} (1 μF cm^{-2}). A channel conducting 1 pA for 1 ms allows 10^{-15} C to pass. This is enough charge to change the potential 100 mV on an area of 10^{-12} m^2 or 1 μm^2. This charge transfer corresponds to about 6000 monovalent ions per μm^2.

Figure 9.12a shows the steady-state potassium and peak sodium current densities for a squid axon. The ion concentrations are known, and we saw in Chap. 6 that the Nernst potentials at 6.3 °C were +50 mV for sodium and −77 mV for potassium. Figure 9.12(b) shows the conductance per unit area, obtained by dividing the current by $v - v_{\text{Nernst}}$. Figure 9.15 shows a semilogarithmic plot of the conductance per unit area.

The sodium current density changes sign at the sodium Nernst potential. While a measured zero crossing is an accurate way to determine the Nernst potential, extrapolation to find the zero-crossing can be quite misleading. The potassium current density appears to be linear over a large region, and it is tempting to extrapolate to find v_K. The extrapolation shows zero current at about −40 mV, which is far from v_K. The reason can be seen in Fig. 9.12(b), which shows that g_K is varying considerably over the region where j_K appears to be linear; this distorts the slope and changes the extrapolated intersection.

A simple two-state model can explain the general shape of the curves in Fig. 9.15. The conductance per unit area of a membrane is the product of the conductance of an open pore and the average number of pores per unit area that are open.

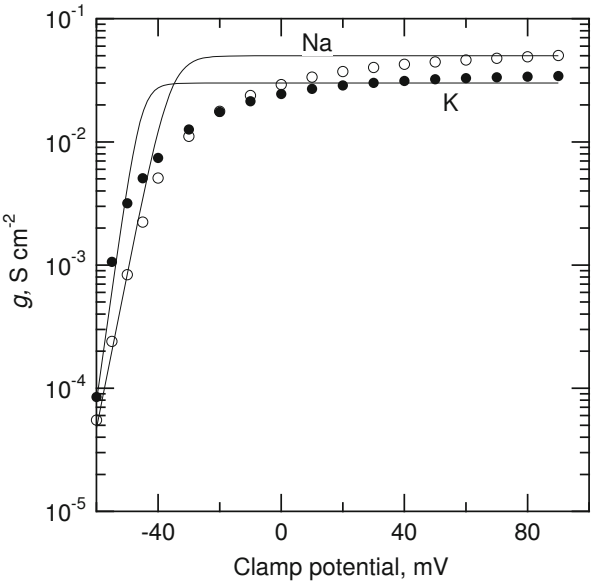

Fig. 9.15 Semilog plot of sodium and potassium conductivities from Fig. 9.12(b) with fits by Eq. 9.57. For sodium $u_o = -10.5$ and $z = -7$; for potassium $u_o = -19$ and $z = -10$

The model assumes that each channel has a gate that is either open or closed. When the gate is open, the channel has a conductance determined by the passive properties of the rest of the channel. The rapid increase of conductance between -60 and -30 mV corresponds to a rapidly increasing probability that the gate is open.

Suppose that each channel has a gate with two states: open and closed. When there is no average electric field in the membrane ($v = 0$), the energy of the open state is $w = u_o k_B T$ greater than the closed state. Suppose also that as the gate opens and closes, a charge q associated with the gate moves a small distance parallel to the axis of the pore. When there is a potential v across the membrane, the charge moves through a potential difference αv, where $\alpha < 1$. The total energy change when the gate opens with potential v across the membrane is then $w + q\alpha v$. The quantity $q\alpha$ is often written as ze and called the *equivalent gating charge*. In terms of $k_B T$, the energy change when the pore opens is $u = u_o + zev/k_B T$.

Let p_o be the probability that a pore is open and p_c be the probability that it is closed. The probabilities are related by a Boltzmann factor: $p_o = p_c e^{-u}$. Since $p_o + p_c = 1$, $p_o = e^{-u}/(1 + e^{-u}) = 1/(1 + e^{u})$,

$$p_o = \frac{1}{1 + e^{u_o + zev/k_B T}}. \tag{9.57}$$

For very large values of u (small values of p_o),

$$p_o \approx e^{-(u_o + zev/k_B T)}. \tag{9.58}$$

The conductance per unit area of the membrane is the conductance of an open pore times the number of pores per unit area (that is g_∞), times p_o. Figure 9.15 shows plots of the "data" and lines generated from Eq. 9.57. The multiplicative constant has been adjusted to fit the flat region of the "data" at high v. Parameters u_o and z have been adjusted to provide good fits at the lowest conductances. For sodium $u_o = -10.5$ and $z = -7$; for potassium $u_o = -19$ and $z = -10$. The fact that u_o is very negative means that when $v = 0$ the energy of an open gate is much less than the energy of a closed gate. Nearly all of the pores are open, as can be seen from the $v = 0$ point in Fig. 9.15. The fact that $z = -7$ or -10 means that when the pore opens or closes the equivalent of 7 (or 10) electron charges must move through the full transmembrane potential difference. Many more charges could be displaced a much smaller distance and experience a much smaller potential change. More sophisticated multilevel models are discussed by Sigworth (1993).

This charge movement constitutes a very small current called the *gating current*. It is different from the current to charge the membrane capacitance. We saw above that during a 1-pA pulse lasting 1 ms, about 6000 monovalent ions flow through the membrane. The gating charge is about 10 monovalent charges, a ratio of about 600. The gating current is so small that it has not yet been measured in a single channel, but it can be measured by manipulating the ions bathing the membrane in a patch-clamp experiment. Figure 9.16 shows the results of a set of experiments with *Shaker* potassium channels. Panel A shows the macroscopic depolarizations to $+20$ and $+80$ mV for a patch with about 400 channels. The peak current at $+80$ mV is 1.25 pA per channel. Panel B shows the gating current recorded from another patch containing about 8000 channels. Potassium was removed from the solution bathing the interior surface of the membrane. The gating current lasts slightly less than 1 ms and peaks at about 4.5×10^{-15} A per channel, about 300 times less than the channel current. The agreement with our first estimate of 600 times less is satisfactory, given the accuracy of the data. Panels C and D show recordings similar to panel A, but with only a few channels in the patch. The results from three successive depolalrizing pulses are shown in each case. The channel openings are similar to those in Fig. 9.13, but are recorded at a much shorter time scale. The increased current through an open channel and the higher probability of being open for a clamp of $+80$ mV are both apparent. The smooth macroscopic current shown in Fig. 9.16a is the sum of many discrete channel currents like those shown in Fig. 9.16c.

A very simple approximate calculation shows that there is not much ion–ion interaction in a channel. A current of 1 pA is 6.25×10^6 monovalent ions per second, so that the average time between the passage of successive ions through the channel is 1.6×10^{-7} s. In a uniform electric field giving

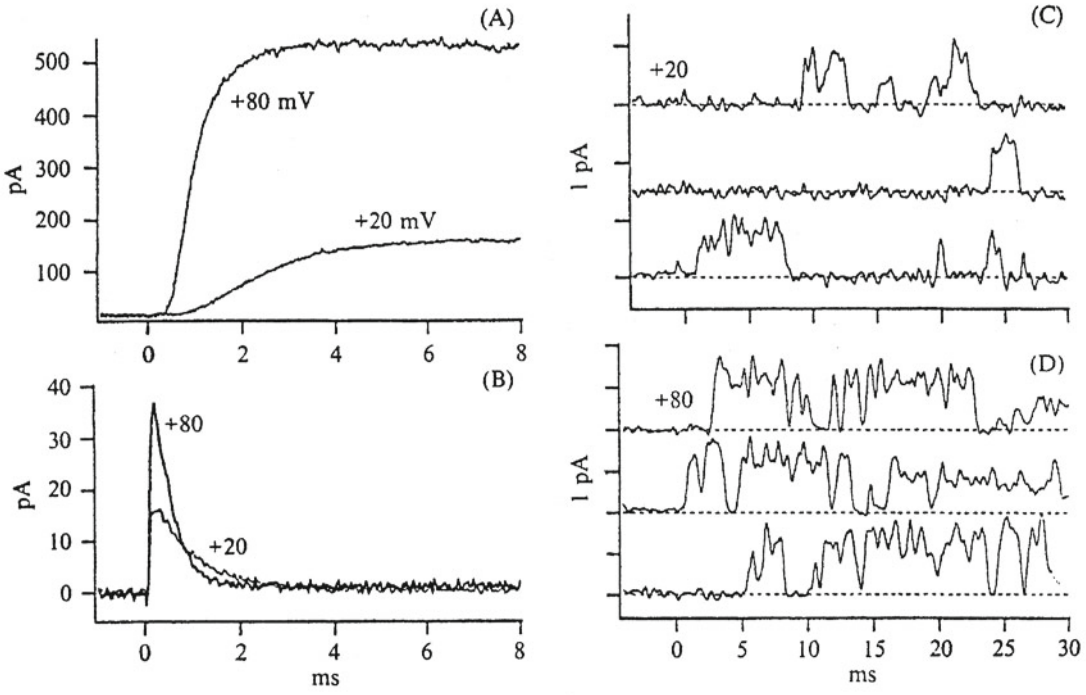

Fig. 9.16 The results of a set of experiments with *Shaker* potassium channels. Panel A shows the macroscopic depolarizations to +20 and +80 mV for a patch with about 400 channels. Panel B shows the gating current recorded from another patch containing about 8000 channels. Potassium was removed from the solution bathing the interior surface of the membrane. Panels C and D show recordings similar to *panel A*, but with many fewer channels in the patch. The results from three successive depolarizing pulses are shown in each case. (From F. J. Sigworth (1993). Reprinted with permission of Cambridge University Press)

80 mV across the membrane, a monovalent ion would have a drift velocity of 0.6 m s^{-1} based on the bulk diffusion constant. (See the discussion surrounding Eq. 4.22.) As ions in the pore are confined, let us use $\frac{1}{10}$ of this, or 0.06 m s^{-1}. (The diffusion constant is proportional to the solute permeability; see Sect. 5.9. Ignoring electric forces, we see from Fig. 5.16 that $\omega/\omega_0 = 0.1$ corresponds to $a/R_p = 0.4$. So this is probably still a high drift velocity.) Then the time it takes the ion to pass through the channel is its length (assume 6 nm) divided by the average speed, or 10^{-7} s. The fraction of the time there is an ion in the channel is $f = 0.625$.

We can make some other estimates of channel parameters. Over some part of its length, the channel must be narrow enough so the wall can interact directly with the ion that is passing through, not shielded by water molecules. The pore must therefore be narrowed to a radius of 0.3 to 0.7 nm in some region. Let us assume a cylindrical pore of radius $a = 0.7$ nm and length $h = 6$ nm. The average number of water molecules in the channel is 308; the average concentration of ions is $f/(\pi a^2 h) = 113$ mmol l^{-1}, which is about right. The resistance of a channel while it is open is $R = v/i = 80$ mV/1 pA $= 8 \times 10^7$ Ω. (We should actually use $v - v_{\text{Nernst}}$, but this is a rough estimate. If we were going to be more accurate, we should also use the Nernst–Planck equation, recognizing that the ions move by diffusion as well as drift.)

9.8 Noise

The current fluctuates while a channel is open, as can be seen in Figs. 9.13 and 9.16. Some of the fluctuation is due to noise in the measurement apparatus. However, there are some fundamental physical lower limits to the fluctuations resulting from noise in the membrane patch itself. We discuss these briefly here, with a more extensive discussion in Chap. 11. DeFelice (1981) wrote an excellent book on noise in membranes.

9.8.1 Shot Noise

The first (and smallest) limitation is called *shot noise*. It is due to the fact that the charge is transported by ions that move randomly and independently through the channels. Imagine a single open conducting channel with an average current $\bar{i}$ of monovalent ions. During time Δt (which can be any interval

shorter than the time the channel is open), the average charge flow is $\bar{i}\Delta t$ and the average number of ions is $\overline{n} = \bar{i}\Delta t/e$. Since there are a very large number of ions that might flow through the channel (occurrences) and the probability that any one ion moves through the channel during Δt is very small, we have the Poisson limit of the binomial distribution (Appendix J). The variance in the number of ions is $\sigma_n^2 = \overline{n} = \bar{i}\Delta t/e$. Since the average charge transported is $\overline{q} = \overline{n}e$, the variance in the charge is $\sigma_q^2 = e^2\sigma_n^2 = e\bar{i}\Delta t$. When many samples of length Δt are measured, the variance in the current is $\sigma_i^2 = \sigma_q^2/(\Delta t)^2$. The standard deviations are

$$\begin{aligned} \sigma_n &= \left(\frac{\bar{i}\Delta t}{e}\right)^{1/2}, \\ \sigma_q &= \left(e\bar{i}\Delta t\right)^{1/2}, \\ \sigma_i &= \left(\frac{e\bar{i}}{\Delta t}\right)^{1/2}, \end{aligned} \tag{9.59}$$

and the fractional standard deviations are

$$\frac{\sigma_n}{\overline{n}} = \frac{\sigma_q}{\overline{q}} = \frac{\sigma_i}{\bar{i}} = \left(\frac{e}{\bar{i}\Delta t}\right)^{1/2}. \tag{9.60}$$

For a current of 1 pA, the fractional standard deviation is 0.013 when the sampling time is 1 ms and 0.04 when the sampling time is 0.1 ms. These are much smaller than what is observed in the figures.

9.8.2 Johnson Noise

The next source of noise is called *Johnson noise*. It arises from thermal fluctuations or Brownian movement of the ions. It can be derived from a microscopic model of conduction (either in an ionic solution or a metal), but we will do it using the equipartition of energy.

First, we need an expression for the energy U contained in a charged capacitor. To obtain it, imagine that an amount of charge $+dq$ is transferred from the negative to the positive conductor. This increases the amount of positive charge on the positive conductor and also increases the amount of negative charge on the negative conductor. The work required to transfer the charge when the potential difference between the conductors is v is vdq. The energy stored in the capacitor is the total work required to charge the conductor from 0 to q. Remembering that $q = Cv$, we have

$$U = \int_0^q v\,dq = \frac{1}{C}\int_0^q q\,dq = \frac{q^2}{2C} = \frac{Cv^2}{2}. \tag{9.61}$$

If the capacitor is completely isolated, there can be a constant charge on each conductor with no fluctuations. If the capacitor is in thermal contact with its surroundings and is in equilibrium, then the equipartition theorem applies. The capacitor can be brought into thermal equilibrium with its surroundings by connecting a resistance R between the conductors. This will discharge the capacitor so $\overline{q} = \overline{v} = 0$. There will be fluctuations around these zero values. As the expression for the energy depends on the square of the variables, the mean square value is given by the equipartition of energy theorem, Eq. 3.38. We will assume that when the capacitor is charged, thermal fluctuations give the same variances as when it is discharged:

$$\sigma_v^2 = \left(\overline{v^2} - \overline{v}^2\right) = \overline{v^2} = k_BT/C, \tag{9.62a}$$

$$\sigma_q^2 = \left(\overline{q^2} - \overline{q}^2\right) = \overline{q^2} = Ck_BT. \tag{9.62b}$$

In a simple RC circuit, $i = v/R$, so

$$\sigma_i^2 = \sigma_v^2/R^2 = k_BT/R^2C. \tag{9.62c}$$

Since changes in current or voltage in an RC circuit occur with time constant $\tau = RC$, we can also write these as

$$\sigma_v^2 = Rk_BT/\tau, \quad \sigma_i^2 = k_BT/R\tau. \tag{9.63}$$

These are special cases of a more general relationship that will be discussed in Chap. 11.

We can use these to determine some of the requirements for patch-clamp recording. In order to see the current from a single channel with some accuracy, let us require that the standard deviation of the current fluctuation be less than $\frac{1}{8}$ of the signal we want to measure. (This signal-to-noise ratio, $SNR = 8$, is arbitrary.) First, consider the limitation due to Johnson noise. We want $\sigma_i < \bar{i}/8$ or $\sigma_i^2 < \left(\bar{i}\right)^2/64$. From this, we obtain

$$R > \left(\frac{k_BT}{C}\right)^{1/2}\frac{8}{\bar{i}}. \tag{9.64}$$

The capacitance of a patch of membrane of 1 μm radius is 3.1×10^{-14} F. At a temperature of 300 K and for an average current of 1 pA, this gives $R > 3 \times 10^9\ \Omega$. Larger values of R will give an even higher SNR. There are several sources of thermal noise in a recording electrode, all discussed in the paper by Hamill et al. (1981). These are order-of-magnitude results; one must determine carefully which capacitances and resistances provide the dominant effects.

We can also see when shot noise is important. The ratio of Johnson noise to shot noise is

$$\frac{\sigma_i^2(\text{Johnson})}{\sigma_i^2(\text{shot})} = \frac{k_BT/R\tau}{e\bar{i}/\Delta t} = \frac{k_BT}{Re\bar{i}}. \tag{9.65}$$

This ratio is less than 1 and shot noise is important when $R > k_BT/e\bar{i} = 2.6 \times 10^{10}\ \Omega$. Shot noise has been detected in channel gating currents and subjected to very sophisticated analysis. See the paper by Crouzy and Sigworth (1993) and the references therein.

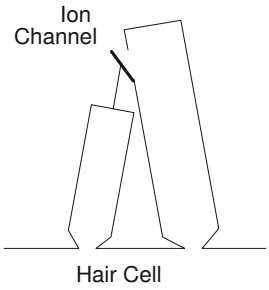

Fig. 9.17 A schematic diagram of two stereocilia linked by a filament that opens a channel as the cillia move back and forth

9.9 Sensory Transducers

Animals have very acute senses. We will see (Problem 13.19) that the ear can hear sounds at 1000 Hz that are just greater than the pressure fluctuations due to molecular collisions on the ear drum. An eye that is adapted to the dark can detect flashes of light corresponding to a few photons (Chap. 14). Many animals can smell chemicals when only a few molecules strike their sensory organs. The electric skate can detect extremely small electric fields. In each case a transducer converts the sensory stimulus into a series of nerve impulses. The transducer must have sufficient sensitivity to respond to the stimulus, and it must also absorb an amount of energy from the stimulus that is greater than what it receives from random thermal bombardment (Brownian movement).[5] We describe here two transducers: the mechanoreceptors (hair cells) of the inner ear and the electric organ of the skate.

Various transduction mechanisms are reviewed in Chap. 8 of Hille (2001). The mechanoreceptors of the bullfrog inner ear have been studied for many years. The hair-cell current rises from 0 to 100 pA with a 0.5-μm displacement. Each hair cell is cylindrical. On its end face are found about 60 very small *stereocilia*, each 1–50 μm long and with a 100–500-nm radius. The tips of these stereocilia are linked by thin filaments. The hair cells and stereocilia that detect sound in the ear are attached to the basilar membrane in the cochlea of the ear and move in a very viscous fluid as the basilar membrane vibrates. Hair cells detecting accelerations of the entire animal are attached to a suspended dense body. It is believed that as the stereocilia move, these filaments pull open flaps at the end of ion channels, allowing ions to enter the cell and initiate the conduction process. This is shown schematically in Fig. 9.17. Denk and Webb (1989) have used a laser interferometer to measure the motion of the hair cells. They found that the spontaneous motion consists primarily of thermal excitation (Brownian motion). Fluctuations in the intracellular voltage were also measured. They often correlated with the motion of the hair cells.

Freshwater catfish respond to electric fields as low as 10^{-4} V m^{-1}. Saltwater sharks and rays can detect fields of 5×10^{-7} V m^{-1}. A brief review has been given by Bastian (1994); Kalmijn (1988) provides a very complete review. The saltwater fish have a more complicated sensory apparatus than the freshwater fish, known as the *ampullae of Lorenzini*. Kalmijn et al. discovered that the ocean flounder generates a current dipole of 3×10^{-7} A m. Sea water with resistivity of 0.23 Ω m gives an electric field of 2×10^{-5} V m^{-1} at a distance 10 cm in front of the flounder. They were able to show in a beautiful series of behavioral experiments that dogfish (a small shark) could detect the electric field 0.4 m from a current dipole of 4×10^{-7} A m, corresponding to an electric field of 5×10^{-7} V m^{-1}. The fish would bite at the electrodes, ignoring a nearby odor source. A field of 10^{-4} V m^{-1} would elicit the startle response. A field $\frac{1}{10}$ as large caused a physiologic response. The animals responded to a constant field or a sinusoidally alternating field up to 4 Hz. At 8 Hz the threshold increased by a factor of 2.

In a series of experiments Lu and Fishman (1994) dissected out the ampulla of Lorenzini and measured its response in the laboratory. They found that the resting rate of firing of the organ is about 35 Hz (impulses per second) and that an applied electric potential increases or decreases the firing rate by about 1 Hz μV^{-1}, depending on its sign. The firing rate saturated for potential differences of 100 μV.

The behavioral experiments showed sensitivity to an electric field of 0.5 μV m^{-1}. The anatomy of the ampulla is such that the organ senses the potential difference between the surface of the fish and deep in its interior. Pickard (1988) shows that for a spherical fish of radius a, this gives a potential of $3aE/2$, where E is the external electric field. The amplitude of the potential difference oscillation of a fish of length $\frac{1}{3}$ m is therefore 0.25 μV. This is enough to cause a 1 % change in firing rate, which could be detected by neuronal circuits (Adair et al. 1998).

The Johnson noise is somewhat smaller than the signal detected. To estimate it, use Eq. 9.62a with the ampullary capacitance of 0.15 μF measured by Lu and Fishman. The standard deviation of the noise is 0.17 μV.

9.10 Possible Effects of Weak External Electric and Magnetic Fields

There is a lingering controversy over whether radio-frequency (cell phone, 450 MHz–2 GHz) and power-line-frequency (50–60 Hz) electric or magnetic fields can cause

[5] For the detection of light, the amount of energy per photon is so much greater than $k_B T$ that shot noise dominates.

cancer. While the effect, if any, is quite small, the literature is extensive, involving both epidemiological and laboratory studies. Results are conflicting, and the mechanisms by which such an effect might occur are not yet understood. Mechanisms have been proposed, some of which are inconsistent with basic physical principles such as the Boltzmann factor, the mean free path of ions, and thermal fluctuations. A review in the physics-teaching literature was provided by Hafemeister (1996).

It is beyond our scope to do more than provide pointers to the field and discuss some basic underlying physics. We consider here the power-line frequencies.

We have seen that electric charges give rise to electric fields, and moving electric charges (currents) generate magnetic fields. The electric field lines start and end on charges, and the magnetic field lines surround the currents. We will see in Chap. 14 that accelerated charges generate electromagnetic *radiation*, in which the electric and magnetic fields are interrelated and the field lines close on themselves far from the source charges. Energy is radiated; it leaves the source and never returns. This radiated energy is in the form of discrete packets or *photons*, whose energy is related to the frequency of oscillation of the fields. The energy of each photon is $E = h\nu$, where h is Planck's constant and ν is the frequency. At room temperature, the energy of random thermal motion is $k_B T = 4 \times 10^{-21}$ J. At 60 Hz, the energy in each photon is much smaller: 4×10^{-32} J. At 100 MHz, it is 7×10^{-26} J. For electromagnetic radiation in the ultraviolet and beyond, which certainly can harm cells, the photon energy is 5×10^{-19} J or greater, quite large compared to $k_B T$. At the very low frequencies we are considering it is the strength of the electric or magnetic field that is important, not the energy of individual photons. A more detailed discussion of the distinction between these low-frequency "near fields" and "radiation fields" is found in Polk (1996).

9.10.1 Strong Fields

Electrical burns, cardiac pacing, and nerve and muscle stimulation are produced by electric or rapidly changing magnetic fields. Even stronger electric fields increase membrane permeability. This is believed to be due to the transient formation of pores (*electroporation*). Pores can be formed, for example, by microsecond-length pulses with a field strength in the membrane of about 10^8 V m^{-1} (Weaver 2000). Microwaves are used to heat tissue. Nerve stimulation requires a few millivolts across the cell membrane, or about 10^5–10^6 V m^{-1}. Both electric and magnetic fields are used to promote bone healing, with field strengths in tissue in the fracture region of 10^{-1} V m^{-1} (Tenforde 1995), though these results are controversial (Adair 2000).

9.10.2 Power Frequency (50–60 Hz) Fields

9.10.2.1 Fields in Homes are Weak

Much weaker fields in homes are produced by power lines, house wiring, and electrical appliances. Barnes (1995) found average electric fields in air next to the body of about 7 V m^{-1}, with peak values of 200 V m^{-1}. (We will find that since the body is a conductor, the fields within the body are much less.) Average residential magnetic fields are about 0.1 μT, with peaks up to four times as large. Within the body they are about the same. Tenforde (1995) reviews both power-line and radio-frequency field intensities.

9.10.2.2 Epidemiological Studies

Epidemiological studies have been very valuable in tracing the cause of infectious outbreaks. They have also indicated that smoking increases the probability of developing lung cancer by 3000 %—a factor of 30. However, there are difficulties with epidemiological studies when the effect is small: there are inescapable statistical fluctuations unless the number of subjects is huge; associations do not prove causality; and there may be unrecognized variables that are confusing the picture. The problem is exacerbated when positive findings receive widespread publicity and negative findings are ignored by the press.

Epidemiological studies usually report *relative risk*: the incidence in an exposed group divided by the incidence in an unexposed group. A relative risk of one means no effect. John Moulder, the author of a web site about power lines and cancer that unfortunately no longer exists, said,

> A strong association is one with a relative risk (RR) of 5 or more. Tobacco smoking, for example, shows a strong association, with the risk of lung cancer in smokers being 10–30 times that of non-smokers. A relative risk of less than about 3 indicates a weak association. A relative risk below about 1.5 is essentially meaningless unless it is supported by other data.
>
> Most of the positive power-frequency studies have relative risks of two or less. The leukemia studies as a group have relative risks of 0.8-1.9, while the brain cancer studies as a group have relative risks of 0.8-1.6. This is a weak association. Interestingly, as the sophistication of the studies has increased, the relative risks have not increased.

One would also expect an increased response with increasing dose. Moulder continued,

> No published power-frequency exposure study has shown a statistically-significant dose-response relationship between measured fields and cancer rates, or between distances from transmission lines and cancer rates. However, there is some indication of a dose-response in some of the older childhood leukemia studies when wire codes or calculations of historic fields are used as exposure metrics. The lack of a clear relationship between exposure and increased cancer incidence is a major reason why most scientists are skeptical about the significance of much of the epidemiology.

9.10.2.3 Laboratory Studies

The many laboratory studies were also reviewed by Moulder. He concluded:

> Power-frequency fields show little evidence of the type of effects on cells, tissues or animals that point towards their being a cause of cancer, or to their contributing to cancer. In fact, the existing laboratory data provides strong evidence that power-frequency fields of the magnitude to which people are exposed are not carcinogenic.[6]

9.10.2.4 Reviews and Panel Reports

Reviews by Moulder and Foster (1995, 1999) find that the association between power-frequency fields and cancer is weak[7] for magnetic fields and even weaker for electric fields. Carstensen (1995) and Bren (1995) reach similar conclusions.

A report by a committee of the National Research Council concludes that

> the current body of evidence does not show that exposure to these fields presents a human-health hazard.... The committee reviewed residential exposure levels to electric and magnetic fields, evaluated the available epidemiological studies, and examined laboratory investigations that used cells, isolated tissues, and animals. (National Research Council (1997), p. 2)
>
> There is no convincing evidence that exposure to 60-Hz electric and magnetic fields causes cancer in animals.... There is no evidence of any adverse effects on reproduction or development in animals, particularly mammals, from exposure to power-frequency 50- or 60-Hz electric or magnetic fields. (National Research Council 1997, p. 7).

9.10.2.5 Electric Fields in the Body

We now review some of the basic principles that govern the interaction of electric and magnetic fields with the body. One of the important principles is the relationship between the electric field in air and the field within the body, which is a conductor. A simple model that shows how this coupling takes place is the one-dimensional problem shown in Fig. 9.18. An infinite slab of tissue has dielectric constant κ and conductivity σ. In the air perpendicular to the surface of the slab is an external oscillating electric field $E(t) = E_0 \cos \omega t$. We assume that the dielectric constant is independent of frequency and accounts for the polarization

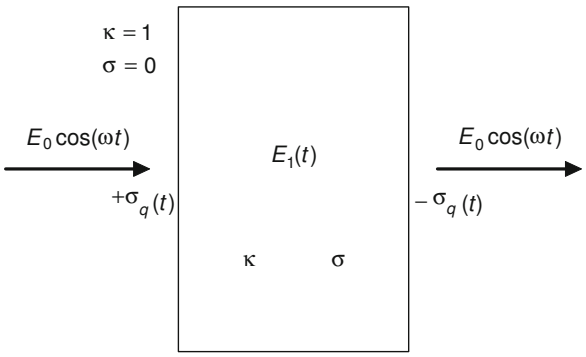

Fig. 9.18 An infinite slab of tissue is immersed in an oscillating electric field of amplitude E_0 in air

of the tissue. An ionic current flows and causes free charge per unit area $\pm\sigma_q$ to accumulate on the surfaces of the slab. Within the slab, the field is $E_1(t)$ and the current density is $j = \sigma E_1$. Gauss's law (Eq. 6.21b) applied to either surface gives

$$-\epsilon_0 E_0 \cos \omega t + \kappa \epsilon_0 E_1(t) = \sigma_q(t). \tag{9.66}$$

Conservation of free charge at the surface requires that[8]

$$\sigma E_1 = j = -\frac{d\sigma_q}{dt}. \tag{9.67}$$

If we differentiate Eq. 9.66 and combine it with Eq. 9.67, we obtain

$$\frac{dE_1}{dt} + \frac{\sigma}{\kappa\epsilon_0} E_1 = -\frac{\omega}{\kappa} E_0 \sin \omega t. \tag{9.68}$$

The factor $\kappa\epsilon_0/\sigma$ is a characteristic of the tissue and has the dimensions of time. We will call it τ_t.[9] Typical tissue conductivity is about 0.1 S m^{-1}. We must be careful about the value of the dielectric constant. We have used a value of 80 for water. However, tissue is much more complex than pure water and there are several effects that alter the dielectric constant (Foster and Schwan 1996). It takes time for both the polarization charges and conducting ions to move. As a result, both the conductivity and the dielectric constant of tissue depend on the frequency of the applied electric field and in fact are not independent of one another (see Foster and Schwan 1996, especially pp. 31–41). Several effects change

[6] Foster (1996) reviewed many of the laboratory studies and described cases where subtle cues meant the observers were not making truly "blind" observations. Though not directly relevant to the issue under discussion here, a classic study by Tucker and Schmitt (1978) at the University of Minnesota is worth noting. They were seeking to detect possible human perception of 60-Hz magnetic fields. There appeared to be an effect. For 5 years they kept providing better and better isolation of the subject from subtle auditory clues. With their final isolation chamber, none of the 200 subjects could reliably perceive whether the field was on or off. Had they been less thorough and persistent, they would have reported a positive effect that does not exist.

[7] That is, the carcinogenic effects are in International Association for Research on Cancer group 2B (possibly carcinogenic), a group that includes coffee and pickled vegetables.

[8] Readers who are familiar with the concepts of reactance and complex impedance must be frustrated because we have not used them. The reason is pedagogic. Because many in our intended audience may have had only one year of calculus, we want to avoid the use of complex numbers. In Chap. 11 we introduce them as a parallel notation. They are widely used in the image reconstruction described in Chap. 12.

[9] Recall that the membrane time constant τ was used in Eq. 6.40. The values of conductivity or resistivity and dielectric constant are different in this case.

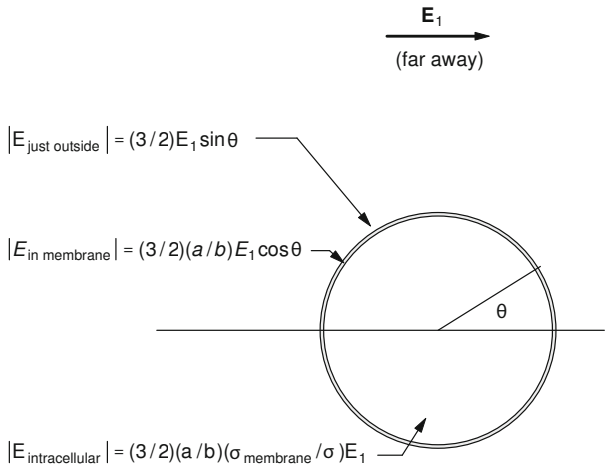

Fig. 9.19 The electric fields in and around a *spherical cell*. The *cell* has radius a and membrane thickness b. The field far from the *cell* has an amplitude E_1

the conductivity and dielectric constant as a function of frequency. At power-line frequencies, the dominant effect is the slight movement of the counterions and charge in the double layer at a cell membrane in response to the applied electric field. As a result, $\kappa \approx 10^6$ and $\tau_t = 9.1 \times 10^{-5}$ s.

We try a solution to Eq. 9.68 of the form $E_1(t) = A \sin \omega t + B \cos \omega t$. It satisfies the equation if

$$A = -\frac{\omega\tau_t}{\kappa(1+\omega^2\tau_t^2)}E_0 \approx -\frac{\omega\epsilon_0}{\sigma}E_0,$$
$$B = -\omega\tau_t A = -\frac{(\omega\tau_t)^2}{\kappa(1+\omega^2\tau_t^2)}E_0 \approx 0. \tag{9.69}$$

For 60 Hz and a dielectric constant of 10^6, $A = 33\times10^{-9}E_0$, $B = 1.1 \times 10^{-9}E_0$. The amplitude of the field in tissue is $E_1 \approx A$:

$$E_1 \approx 33 \times 10^{-9}E_0. \tag{9.70}$$

The field in air is reduced by a factor of about 3×10^{-8} in tissue because the tissue is a good conductor. The total reduction is nearly the same for a dielectric constant of 80, as can be seen from the fact that the approximate form for A does not depend on κ.

9.10.2.6 Electric Fields in a Spherical Cell

Another important factor is the electric fields that exist in and near a cell. Consider a spherical cell with inner radius a and membrane thickness b immersed in an infinite conducting medium in which there is an electric field E_1 far from the cell. We saw above that a field in air of $E_0 = 300$ V m^{-1} is reduced to $E_1 = 10^{-5}$ V m^{-1} in the conducting medium. The potential can be determined analytically by solving Poisson's equation (with zero charge density) in the three regions and matching boundary conditions much as we did to obtain Eq. 9.67. The results, valid for slowly varying applied fields such as a 50 or 60-Hz power line field, are shown in Fig. 9.19.[10] Only the amplitude of the electric field is shown. Assume the conductivities σ of the extracellular and intracellular fluids are the same, that $a = 10$ μm and $b = 6$ nm, and that $\sigma_{\text{membrane}} = 2.4 \times 10^{-8}\sigma$. The important features of this solution are that the field just outside the cell is roughly the same as the field far away, the field inside the membrane is magnified by a large factor (a/b), and the field inside the cell is multiplied by a very small factor $(a\sigma_{\text{membrane}}/b\sigma)$. Thus, the cell membrane shields the intracellular space from extracellular electric fields, so these fields are not likely to directly affect cell organelles and important biomolecules such as DNA. This is reflected in the last line of Table 9.5.

Table 9.5 Comparison of the signal in a cell to thermal noise for an applied electric field in air $E_0 = 300$ V m^{-1}. From Eq. 9.71, $E_1 = 10^{-5}$ V m^{-1}. $T = 300$ K. $z = 10$. $d = 10^{-5}$ m

Model	Outside the cell	In the cell membrane	Inside the cell
E (V m^{-1})	1.0×10^{-5}	1.62×10^{-2}	5.40×10^{-10}
k_BT/eE (m)	2.57×10^{3}	1.59	4.79×10^{7}
$zeEd/k_BT$	3.9×10^{-8}	6.3×10^{-5}	2.1×10^{-12}

9.10.3 Electrical Interactions and Noise

If an organism is affected in some way by an external field, then it can be regarded as a detector of that field. The external field can therefore be thought of as a signal. To be detected, the signal must be greater than the noise. The noise can be either thermal (Johnson) noise, shot noise, or noise from the electric currents that normally flow in the body due to nerve conduction and muscle contraction. To have a signal that is not masked by Johnson noise, we must have an electric field E such that

$$\frac{zev}{k_BT} = \frac{zeEd}{k_BT} > 1, \tag{9.71}$$

where z is the valence of an effective charge that moves a distance d in the electric field E. Table 9.5 shows the result of a calculation using a field in air of 300 V m^{-1}. We use a value $z = 10$. For d, we use the diameter of the cell, $d = 10$ μm (though for the membrane perhaps the much smaller thickness of the cell membrane should be used). The values of $zeEd/k_BT$ are very small.

One proposal to overcome this signal-to-noise problem is that the biological effect is due to the averaging of the field over many cells or over time. This was first proposed by Weaver and Astumian (1990), and a specific model has been

[10] Calculated using equations in Polk (1995), p. 62.

formulated by Astumian et al. (1995). The model applies the Nernst–Planck equation (Eq. 9.37) and shows that if the concentration of some substance outside the cell is much larger than inside, the response to an oscillating v is "rectification" or a net inward current. This would allow an accumulation of the substance within the cell. The averaging times in their model are 13 h. Weaver and Astumian (1995) review the entire causality problem, including the effects of shot noise. Adair (2000) reviews many other aspects of the problem.

9.10.4 Magnetic Interactions and Noise

The magnetic field is not attenuated at the body surface like the electric field is. Kirschvink et al. (1992a) reported that the human brain contains several million magnetosomes per gram. Kobayashi et al. (1995) found that contamination with magnetic particles could affect laboratory experiments with cell cultures, even if the cells being studied do not normally contain magnetosomes. Commercial disposable, presterilized plastic laboratory ware used in tissue culture experiments was found to contain ferromagnetic particles smaller than 100 nm that are readily taken up by white blood cells.

What about the signal-to-noise ratio for magnetic effects? The situation is somewhat more favorable than for the electric case. We saw in Chap. 8 that a single magnetosome has appreciable alignment with the earth's magnetic field, even in the presence of thermal bombardment. The earth's field is about 5×10^{-5} T. For a single magnetosome

$$\frac{m B_{\text{earth}}}{k_B T} = \frac{(6.4 \times 10^{-17})(5 \times 10^{-5})}{(1.38 \times 10^{-23})(300)} = 0.77. \qquad (9.72)$$

For a larger magnetosome of radius 100 μm, $m = 2 \times 10^{-15}$ A m^2 and the energy ratio in the earth's field is 24. The field due to a typical power line is about 100 times smaller: about 2×10^{-7} T.

Kirschvink (1992) proposed a model whereby a magnetosome in a field of 10^{-4}–10^{-3} T could rotate to open a membrane channel. As an example of the debate that continues in this area, Adair (1991, 1992, 1993, 1994) argued that a magnetic interaction cannot overcome thermal noise in a 60-Hz field of 5×10^{-6} T. However, Polk (1994) argued that more biologically realistic parameters, including a large number of magnetosomes in a cell, could allow an interaction at 2×10^{-6} T.

The essential features of all the models are like this. Imagine a particle with magnetic moment **m** in the earth's field. It will tend to align with the field as shown in Fig. 9.20(a). The direction of the magnetic moment with the earth's field is θ. Apply an alternating field $B_0 \cos \omega t$ at right angles to the earth's field, as shown in Fig. 9.20(b). There are three

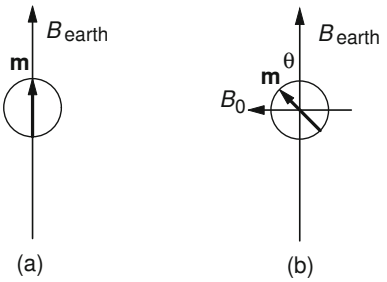

Fig. 9.20 A particle with magnetic moment **m** a aligned with the earth's magnetic field and **b** at an angle θ with the earth's field because of an applied field B_0

torques on the particle. The first is viscous drag, which is proportional to the angular velocity of the particle $d\theta/dt$ but in the opposite direction. The second is the torque tending to align **m** with the earth's field, $-m B_{\text{earth}} \sin\theta$. The third tends to align **m** with the alternating field, $m B_0 \cos \omega t \cos\theta$. Assume that the acceleration is so small that the particle is in rotational equilibrium. (This is not necessary, but it simplifies the math.) Then, from Eq. 1.4,

$$-\beta \frac{d\theta}{dt} + m B_{\text{earth}} \sin\theta - m B_0 \cos \omega t \cos\theta = 0. \qquad (9.73)$$

In order to linearize the equation, assume that θ is small enough so that $\sin\theta \approx \theta$ and $\cos\theta \approx 1$. The linearized equation is

$$\beta \frac{d\theta}{dt} - m B_{\text{earth}} \theta = -m B_0 \cos \omega t. \qquad (9.74)$$

This is a linear differential equation with constant coefficients that can be solved by the techniques of Appendix F. Consider only the particular solution and try a solution of the form

$$\theta = \theta_1 \cos \omega t + \theta_2 \sin \omega t. \qquad (9.75)$$

Substitution of this in the equation shows that

$$\theta_1 = \frac{m^2 B_0 B_{\text{earth}}}{(\omega\beta)^2 + (m B_{\text{earth}})^2},$$

$$\theta_2 = -\frac{\omega\beta m B_0}{(\omega\beta)^2 + (m B_{\text{earth}})^2},$$

and

$$\theta_m = \frac{m B_0}{\left[(\omega\beta)^2 + (m B_{\text{earth}})^2\right]^{1/2}}, \qquad (9.76)$$

where θ_m is the maximum amplitude: $\theta_m^2 = \theta_1^2 + \theta_2^2$. We saw in Chap. 4 (Stokes' law) that the translational viscous drag on a spherical particle is $6\pi\eta a v$. Similarly, the viscous torque on a rotating sphere is $8\pi\eta a^3 (d\theta/dt)$ (Lamb 1932, pp. 588-589). The measured values for viscosity inside a cell range

from 0.003 to 0.015 N s m^{-2} (Polk 1994). Using the average of these, $\beta = 0.009(8\pi)a^3 = 0.23a^3$. The magnetic moment of a single-domain magnetosome is also proportional to volume: $m = 2 \times 10^6 a^3$. This leads to a maximum amplitude that is independent of a:

$$\theta_m = \frac{2 \times 10^6 a^3 B_0}{\left[(377)^2(0.23)^2 a^6 + (2 \times 10^6)^2(5 \times 10^{-5})^2 a^6\right]^{1/2}} = 1.5 \times 10^4 B_0. \quad (9.77)$$

Kirschvink originally argued from data about hair-cell deformation that a deflection of 16° or 0.3 rad is needed. This would require $B_0 = 2 \times 10^{-5}$ T. (He had a slightly different value because he used a different viscosity. He also included the torque due to the force on the channel gate.)

In the absence of the applied field, the thermal fluctuations in angle can be estimated as follows. In the linear approximation, the work required to displace the particle an amount θ from the direction of the earth's field is

$$W = \int \tau \, d\theta = \int m B_{\text{earth}} \theta \, d\theta = m B_{\text{earth}} \frac{\theta^2}{2}. \quad (9.78)$$

Equipartition of energy again gives us

$$\overline{\theta^2}_{\text{thermal}} = \frac{k_B T}{m B_{\text{earth}}} = \frac{k_B T}{(2 \times 10^6)(5 \times 10^{-5}) a^3} = \frac{k_B T}{100 a^3}. \quad (9.79)$$

For a 50-nm magnetosome, this gives $\theta_{\text{rms}} = 0.58$ rad. For a 100-nm magnetosome it is 0.2 rad, comparable to the maximum angles deduced from the model in the preceding paragraph.

9.10.5 Microwaves, Mobile Phones, and Wi-Fi

Many of the concerns about the effects of power-line fields on the body also apply to radio-frequency fields. Sources include radio waves, microwaves, mobile phones, and Wi-Fi devices. A sample of the controversy surrounding this issue can be found in Khurana et al. (2008)[11]

A review by Moulder et al. (2005) concluded that "Overall, a weight-of-evidence evaluation shows that the current evidence for a causal association between cancer and exposure to RF energy is weak and unconvincing." However, they pointed out that there have been only a few epidemiological studies (which overall show no association). Moreover, the energy deposited in a small region of the head by a cell phone may be only an order of magnitude less than the exposure guideline (10 W m^{-2}). While the studies they review did not suggest that RF energy is a primary carcinogen, they could not rule out the possibility that RF energy could enhance the carcinogenicity of other agents.

An exhaustive (390 page) report has been prepared by the International Committee on Non-ionizing Radiation Protection (Vecchia et al. 2009). They point out that heating of tissue by RF energy is well understood. The plausibility of effects by nonthermal mechanisms that have been proposed is very low. Epidemiological studies at the time of publication "give no convincing evidence of a causal relation between RF exposure and any adverse health effect." However, "these studies have too many deficiencies to rule out an association." As for mobile phone use and brain tumors, "overall the studies published to date do not demonstrate a raised risk within approximately 10 years of use for any tumor of the brain or any other head tumor." "For slow-growing tumors... the current observation period is still too short. Currently data are completely lacking on the potential carcinogenic effects of exposures in childhood or adolescence."

Sheppard et al. (2008) evaluated all the proposed mechanisms for radio-frequency interactions with biological molecules and processes They concluded, "an examination of all generally accepted and proposed mechanisms open to quantitative analysis shows that in the frequency range from several megahertz to a few hundred gigahertz, the focus of this paper, the principal mechanism for biological effects, and the only well-established mechanism, is the heating of tissues by dielectric and resistive loss."

In recent years, the use of Wi-Fi to connect computers and household appliances to the Internet has become common. It has become a public concern about possible health effects, particularly in schools. Foster and Moulder (2013) reviewed the current state of research. They concluded that the levels of RF exposure in a house are far below international and US limits. The engineering aspects are well understood. The biological studies are difficult to interpret "but provide no basis to anticipate any biological effects...." They observe

> Finally, it is noted that Wi-Fi and WLANs[12] can raise immediate and urgent safety issues apart from possible RF bioeffects [such as]... privacy invasion and hacking. The Internet... raises a number of safety issues (particularly with children) that have nothing to do with RF exposure. Excessive concern about speculative hazards from RF exposures to Wi-Fi, without concern for these more immediate potential hazards, is comparable to worry about the health effects of using mobile phones without concern for the hazards of texting while driving.

[11] Each issue of the journal *Medical Physics* contains one Point/Counterpoint article, in which a proposition is stated and two prominent medical physicists debate it, one for and one against. You can download all the point/counterpoint articles at http://www.medphys.org. They are a great resource to use when teaching medical physics.

[12] Wireless local area networks.

Symbols Used in Chapter 9

Symbol	Use	Units	First used page
a	Radius	m	245
b	Spacing	m	245
d	Displacement of charge	m	259
e	Electron charge	C	239
f	Force	N	247
f	Fraction of time an ion is in a channel		254
g_{K}	Potassium conductance per unit area	S m^{-2}	252
h	Length of cylindrical channel	m	254
h	Planck's constant	J s	257
j, $\overline{j}$	Electric current density	A m^{-2}	248
j_s	Particle current density	m^{-2} s^{-1}	247
j_v	Volume current density	m s^{-1}	247
k_B	Boltzmann constant	J K^{-1}	239
$\mathbf{m}$	Magnetic moment	A m^2	260
n	Number of ions		254
p_e, $\mathbf{p}_e$, p_{tot}	Electric dipole moment	C m	246
p, p_c, p_o	Probability		253
q	Charge	C	245
r, $\mathbf{r}$	Position	m	241
r	Radius in cylindrical coordinates	m	249
r	Radius in spherical coordinates	m	244
t	Time	s	254
u	$rv(r)$	V m	244
u, u_o	Energy (normalized to k_BT)		248
v, v'	Potential	V	239
v_{Nernst}	Nernst potential	V	248
w	Energy	J or eV	253
x	Position	m	241
x	Distance along cylindrical axis	m	249
z	Valence		239
A, B, A', B'	Constants	V	243
B_{earth}	Earth's magnetic field	T	260
B_0	Amplitude of applied oscillating magnetic field	T	260
C, C'	Concentration	m^{-3}	239
C_i	Concentration of species i	m^{-3}	242
[Cl], [Cl$'$]	Chloride concentration	m^{-3}	240
C	Capacitance	F	255
D, D_{eff}, D_0	Diffusion constant	m^2 s^{-1}	247
E, E_x, E_0, E_1	Electric field	V m^{-1}	241
E_{ext}	External electric field	V m^{-1}	246
E_{pol}	Polarization electric field	V m^{-1}	246
E	Photon energy	J	257
F	Faraday constant	C mol^{-1}	239
F, $\mathbf{F}$	Force	N	247
G	Conductance	S	247
J	Current per unit area of membrane	A m^{-2}	249
[K], [K$'$]	Potassium concentration	m^{-3}	240
L	Separation	m	247
[M$^+$], [M$^{+\prime}$]	Concentration of impermeant cations	m^{-3}	240
[M$^-$], [M$^{-\prime}$]	Concentration of impermeant anions	m^{-3}	240
[M], [M$'$]	Net concentration of impermeant ions	m^{-3}	240
N	Number per unit volume	m^{-3}	246
N_A	Avogadro's number	mol^{-1}	246
[Na], [Na$'$]	Sodium concentration	m^{-3}	240
P	Polarization	C m^{-2}	246
R	Gas constant	J K^{-1} mol^{-1}	239
R	Resistance	Ω	247
R_p	Pore radius	m	249
S	Area	m^2	241
T	Temperature	K	239
U, W	Energy	J	255
V	Particle velocity	m s^{-1}	247
α	Proportionality constant		253
β	Linear viscous drag coefficient	N s m^{-1}	247
β	Rotational viscous drag coefficient	N s m	260
ϵ_0	Electrical permittivity of free space	C^2 N^{-1} m^{-2}	241
κ	Dielectric constant		241
η	Coefficient of viscosity	Pa s	260
λ_D	Debye length	m	242
λ	Characteristic length	m	248
ν	Frequency	Hz or s^{-1}	257
ρ, ρ_{ext}	Charge density	C m^{-3}	241
ρ	Resistivity	Ω m	247
σ_q, σ_q'	Charge per unit area	C m^{-2}	246
σ	Conductivity	S m^{-1}	247
σ_i	Standard deviation of current	A	255
σ_n	Standard deviation of number of ions		255
σ_q	Standard deviation of charge	C	255
σ_q	Charge per unit area	C m^{-2}	258
σ_v	Standard deviation of voltage	V	255
τ	Time constant	s	247
$\boldsymbol{\tau}$	Torque	N m	261
τ_t	Tissue time constant	s	258
θ	Angle		260
ϕ	Angle in cylindrical coordinates		249
χ	Susceptibility		246
ω, ω_s, ω_0	Solute permeability	N^{-1} s^{-1}	249
ω	Angular frequency	s^{-1}	258
ω_t	Characteristic angular frequency of tissue	s^{-1}	
ξ	Energy in units of k_BT		242
Γ	Radial concentration factor		249

Problems

Section 9.1

Problem 1. The chloride ratio between plasma and interstitial fluid is 0.95. Plasma protein has a valence of about -18. In the interstitial fluid, $[\mathrm{Na}'] = [\mathrm{Cl}'] = 155$ mmol l^{-1}. Find the sodium, chloride and protein concentrations in the plasma and the potential difference across the capillary wall, assuming Donnan equilibrium.

Problem 2. Suppose that there are two compartments with equal volume $V = 1$ l, separated by a membrane that is permeable to K and Cl ions. Impermeant positive ions have a concentration 0 on the left and $[\mathrm{M}'] = [\mathrm{M}^{+\prime}] = 10$ mmol l^{-1} on the right. The initial concentration of potassium is $[\mathrm{K}_0] = 30$ mmol l^{-1} on the left. $T = 310$ K.

(a) Find the initial concentrations of potassium and chloride on both sides and the potential difference.

(b) A fixed amount of potassium chloride (10 mmol) is added on the left. After things have come to equilibrium, find the new concentrations and potential difference.

Problem 3. The extracellular space in cartilage contains large, immobile, negatively charged molecules called glycoaminoglycans (GAGs). An early sign of osteoarthritis is the loss of GAGs. The concentration of the GAGs is difficult to measure directly, but Shapiro et al. (2002) measured the sodium ion concentration in cartilage using magnetic resonance imaging (see Chap. 18). Assume the interstitial fluid of the body consists of 150 mM of sodium ions and 150 mM of chloride ions, and that both of these ions can move freely between the body fluid and the extracellular space of cartilage. The cartilage sodium ion concentration is measured to be 250 mM. If Donnan equilibrium holds, what is the concentration of the GAGs? For simplicity, assume the GAGs are monovalent.

Section 9.2

Problem 4. Derive the Poisson equation from Gauss's law in Cartesian coordinates in three dimensions.

Problem 5. Consider ions uniformly dispersed in a solution. Find the average linear separation of the ions for concentrations of 1, 10, 100, and 1000 mmol l^{-1}.

Problem 6. Verify Eq. 9.19.

Problem 7. Verify the parameters presented in Table 9.2. How accurate is the approximation $e^x \approx 1 + x$ in this case?

Problem 8. Consider a solution consisting of an equal concentration, C, of monovalent cations and anions.

(a) Show that $\rho_{\mathrm{ext}} = -2Ce \sinh\left(\frac{ev}{k_B T}\right)$.

(b) Let $\xi = ev/k_B T$ and $\mathbf{r}' = \mathbf{r}/\lambda_D$, where λ_D is given by Eq. 9.13. Show that the nonlinear Poisson–Boltzmann equation (Eq. 9.12) becomes $\nabla'^2 \xi = \sinh \xi$.

Problem 9. Analytical solutions to the nonlinear Poisson–Boltzmann equation are rare but not unknown. Consider the case when the potential varies in one dimension (x), the potential goes to zero at large x, and there exist equal concentrations of monovalent cations and anions. Chandler et al. (1965) showed that the solution to the 1-D Poisson–Boltzmann equation, $d^2\xi/dx'^2 = \sinh \xi$ (see Problem 8), is $\xi(x') = 4 \tanh^{-1}\left[\tanh(\xi_0/4)\, e^{-x'}\right]$, where ξ_0 is a constant and $0 < x' < \infty$.

(a) Verify that this expression satisfies $d^2\xi/dx'^2 = \sinh \xi$. (You may need a math handbook with a collection of hyperbolic function identities.)

(b) Linearize the Poisson–Boltzmann equation and show that its solution is $\xi(x') = \xi_0 e^{-x'}$.

(c) Show that both solutions are equal to ξ_0 at $x' = 0$ and equal to 0 at $x' = \infty$.

(d) Compare the solutions for the linear and nonlinear Poisson–Boltzmann equation at $x' = 0.5$ for the cases $\xi_0 = 0.1$, 1, and 10.

Section 9.3

Problem 10. The value of A used to obtain Eq. 9.29 was determined by saying that as $r \to 0$, the electric field must approach $ze/\kappa 4\pi\epsilon_0 r^2$. An elaboration of the model would be to say that the central ion has radius a and that the electric field at $r = a$ must be the same as the field at the surface of the ion, $ze/\kappa 4\pi\epsilon_0 a^2$. How does this change the expression for $v(r)$?

Problem 11. Using the method in Sect. 9.3, derive the Poisson–Boltzmann equation in cylindrical coordinates (r, ϕ, z; see Appendix L) assuming the electric field is radial and does not depend on ϕ or z. Solutions to the linearized version of this equation are zeroth order modified Bessel functions (see Abramowitz and Stegun 1972).

Section 9.4

Problem 12. A collection of molecular electric dipoles, each of moment $\mathbf{p}$, are in thermal equilibrium at temperature T. If the dipoles experience an electric field of strength E, then determine the average value of $\cos\theta$, where θ is the angle between the dipole and the electric field. Hint: assume the dipole orientations follow the Boltzmann distribution, which in this case is $\exp(pE\cos\theta/k_B T)$, and integrate over all solid angles $d\Omega = 2\pi \sin\theta d\theta$. Show that if $pE \ll k_B T$ the average of $\cos\theta$ is proportional to E, but if $pE \gg k_B T$

the average of $\cos\theta$ saturates at a value of one. Interpret this physically.

Problem 13. If Fig. 9.7 shows the water molecule in its average orientation, is the central ion an anion or a cation?

Section 9.5

Problem 14. Find an expression for the slope of the Nernst–Planck constant-field curve in Fig. 9.10 when v is equal to the Nernst potential, v_0. Hint: expand the exponentials in Eq. 9.45 around v_0.

Problem 15. Show that when $j = 0$, Eq. 9.42 gives $C(x) = C_0 e^{-zev(x)/k_BT}$, as we already know must be true in equilibrium. Hint: solve for dv/dx.

Problem 16. Calculate the conductivity of saline (9 g of NaCl in 1 l of water) at 25 °C.

Problem 17. The discussion surrounding Eqs. 9.34–9.41 was for a model of ions in a pore with constant electric field. It is also possible to write an integral version of the Nernst–Planck equation. Consider a single channel in which the current is the same for all values of x, the distance along the channel. If the diffusion constant and cross-sectional area of the channel are allowed to vary, and with the usual substitution $u(x) = zev(x)/k_BT$, Eq. 9.41 becomes

$$i = j(x)S(x) = -zeD(x)S(x)\left(\frac{dC}{dx} + C(x)\frac{du}{dx}\right).$$

(a) Show that if each term is multiplied by e^u, this can be written as

$$\frac{ie^{u(x)}}{D(x)S(x)} = -ze\left(e^{u(x)}\frac{dC}{dx} + C(x)e^{u(x)}\frac{du}{dx}\right).$$

(b) Show that if the integration is carried from x_1 to x_2, then the current in the channel is

$$i = -\frac{ze\left[C(x_2)e^{u(x_2)} - C(x_1)e^{u(x_1)}\right]}{I},$$

where the integral

$$I = \int_{x_1}^{x_2} \frac{e^{u(x)}\,dx}{S(x)D(x)},$$

contains all the information about the channel.

Problem 18. Cardiac cells have a potassium channel, called "I_{K1}", which shows inward rectification (larger current for potentials more negative than the potassium Nernst potential, v_K, than for potentials more positive than v_K). This channel sometimes is said to show *anomalous rectification*. Why is it anomalous? (The mechanism of anomalous rectification is described by Nichols et al. 1996.)

Section 9.6

Problem 19. Consider a channel that is 100 times more permeable to potassium than to sodium (ignore all other ions).

(a) Write an equation for the reversal potential as a function of the intracellular and extracellular sodium and potassium ion concentrations.

(b) Assume $[K_i] = 150$, $[Na_i] = 50$, and $[Na_e] = 150$ mM. Plot v_r versus $[K_e]$ using semilog paper. On the same plot, draw the potassium Nernst potential as a function of $[K_e]$.

Problem 20. Calculation of the permeability ratios from measurement of the reversal potential is difficult because the concentrations inside the axon are not known. One can overcome this by measuring how the reversal potential (Eq. 9.55) changes as outside concentrations are varied. Obtain an equation for the shift of reversal potential if two measurements are made: one in which $[Na_1] = 0$, and the other with $[K_1] = 0$ (assume $\omega_{Cl} = 0$).

Section 9.7

Problem 21. A patch–clamp experiment shows that the conductance of a single Ca^{2+} channel is $G = 25$ pS. The membrane thickness is $b = 6$ nm. Use $v = 50$ mV.

(a) Assuming that the resistivity of the fluid in the channel is $\rho = 0.5\ \Omega$ m, find an expression and numerical value for the channel radius a.

(b) If the conductance per unit area is 1200 S m^{-2}, find the number of pores per unit area.

(c) The current is $i = Gv$, where v is the applied voltage. Find an expression for n, the number of calcium ions per second passing through the channel, in terms of whichever of parameters G, v, b, and a are necessary.

(d) How many calcium ions are in the channel at one time, if the calcium concentration is C mmol l^{-1}?

Problem 22. A potassium channel might have a radius of 0.2 nm and a length of 6 nm. If it contained potassium at a concentration of 150 mmol l^{-1}, how many potassium ions on average would be in the channel?

Problem 23. How long does it take for a sodium ion to drift in the electric field (assumed constant) through a membrane of thickness L and applied potential v? How long does it take to move by pure diffusion? Find numerical values when the membrane is 6 nm thick and potential difference is 70 mV.

Problem 24. Suppose that a sodium pore when open passes 10 pA and $j_{Na} = 0.2$ A m^{-2}. Calculate the number of open pores per unit area and the average linear spacing between them.

Problem 25. Calculate the current density of sodium ions in a region of length 6 nm due to (a) pure diffusion when

there is no potential difference and the concentrations are 145 and 15 mmol l^{-1}, (b) pure drift when the concentration is 145 mmol l^{-1} and the potential difference is 70 mV, and (c) both diffusion and drift if the electric field is constant.

Problem 26. Patch-clamp recording is done with a micropipette of radius 1 μm.

(a) If the pipette encircles a single channel with conductance 20 pS, what is the channel current when the channel is open and the voltage across the membrane is 20 mV away from the Nernst potential for the ion in question? Make a simple estimate using Ohm's law.

(b) Assuming a capacitance of 0.01 F m^{-2}, what current charges the capacitance of the membrane patch under the micropipette if a 20-mV change occurs linearly in 5 μs?

Problem 27. The following circuit illustrates the effects that must be considered when an electrode is used to measure the properties of a patch of membrane. R_1 is the resistance of the electrode. R_2 and C are properties of the membrane. The applied voltage $v_0(t)$ is a step at $t = 0$. The electrode current is $i(t)$. The voltage across the membrane patch is $v(t)$.

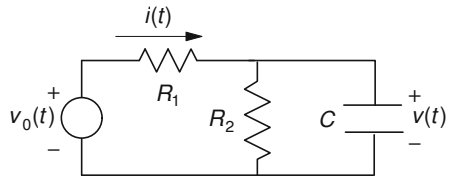

(a) Show that

$$v_0(t) = R_1 C \frac{dv}{dt} + \frac{R_1 + R_2}{R_2} v(t).$$

(b) Show that the time constant is $\tau = R_1 R_2 C/(R_1 + R_2)$ and that $\tau \to R_1 C$ if $R_1 \ll R_2$, $\tau \to R_2 C$ if $R_1 \gg R_2$.

(c) If $v_0(t)$ is a step of height v_0 at $t = 0$, show that

$$v(t) = v_0 \frac{R_2}{R_1 + R_2} \left(1 - e^{-t/\tau}\right)$$

and

$$i(t) = \frac{v_0}{R_1 + R_2} \left(1 + \frac{R_2}{R_1} e^{-t/\tau}\right).$$

(d) Plot $v(t)$ and $i(t)$.

(e) The case $R_1 \ll R_2$ is called *voltage-clamped*. Find expressions for $v(t)$ and $i(t)$ in that case and plot them. Where does the transient current flow? For fixed R_2, what is the time constant?

(f) In the *current-clamped* case, $R_1 \gg R_2$ and $i_0 = v_0/R_1$. Find expressions for $v(t)$ and $i(t)$ and plot them. For fixed R_2, what is the time constant?

(g) Make numerical plots of $v(t)$ and $i(t)$ when $v_0 = 150$ mV, $R_1 = 10^6\ \Omega$, $C = 5$ pF, and $R_2 = 10^{11}\ \Omega$.

Problem 28. A patch-clamp experiment is done with a micropipette having a resistance of $10^6\ \Omega$. When 150 mV is applied across the membrane, the current is 0 when the pores are closed and 1 pA when one channel is open. The membrane capacitance is 4×10^{-3} F m^{-2}. The microelectrode tip has an inner radius of 20 μm. What is the time constant for voltage changes? Does it depend on whether the channel has opened or closed?

Section 9.8

Problem 29. Weaver and Astumian (1990) derived Eq. 9.62a for the thermal noise of the transmembrane potential using a different method than in Sect. 9.8. A resistor has a voltage noise spectral density, $\sigma_e^2(f)$ (in units of V^2 Hz^{-1}), such that $\sigma_e^2(f) = 4k_B T R$, where f is the frequency (Sect. 11.16). It corresponds to voltage e in the figure. Weaver and Astumian represented the membrane as a parallel combination of membrane capacitance C and membrane resistance R (which is always in series with its noise source, e). The voltage across the capacitor, v, is the transmembrane potential.

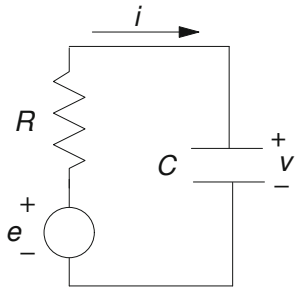

(a) For a particular frequency f, derive a relationship between the spectral density of the voltage fluctuations of the transmembrane potential, $\sigma_v^2(f)$, and $\sigma_e^2(f)$. (Hint: derive an equation governing the voltage in an RC circuit, and then solve it using the methods described in Appendix F.)

(b) Integrate $\sigma_v^2(f)$ over all frequencies to get the voltage fluctuations σ_v^2.

(c) Estimate $\sqrt{\sigma_v^2}$ for a spherical cell of radius 10 μm, having a membrane capacitance per unit area of 0.01 F m^{-2}.

Section 9.9

Problem 30. In some nerve membranes a region of *negative resistance* is found, in which the current decreases as the voltage is increased.

(a) Where have we seen this behavior before?

(b) To see why it happens, consider two cases. The current through the membrane is given by $j = g(v)(v - v_0)$, where $g(v)$ is a property of the membrane, and the Nernst potential v_0 depends on the ion concentration on either side of the membrane. For this problem let

$v_0 = +50$ mV. Calculate j as a function of v for two cases: (a) $g(v) = 1$; (b) the conductance increases rapidly with voltage: $g(v) = (5.6 \times 10^{-7})e^{0.288v}$ (v in mV).

(c) Negative resistance increases the sensitivity of the ampullae of Lorenzini, as measured by Lu and Fishman (1994). To see why, calculate the output voltage in a two-resistance voltage divider network (as in Fig. 6.23) and discuss what happens if R_2 is negative.

Section 9.10

Problem 31. Estimate the transmembrane potential that corresponds to the threshold for electroporation. Compare it to the normal cell resting potential.

Problem 32. Here is one way that signal-to-noise ratio can be improved. Suppose that there are N receptors, connected in the nervous system in such a way that an output response requires a logical AND between all N receptors. The output is sampled every t seconds to determine whether or not there is a response. If the signal exists, all N receptors respond. If the signal does not exist, each receptor responds to thermal noise with a probability p (which might be $p = e^{-U/k_BT}$, where U is an activation energy). Assume that p is the same for each receptor, and that whether a receptor has responded to thermal noise is independent of the response of all other receptors and also independent of its response at any other time.

(a)What is the signal-to-noise (S/N) ratio as a function of N? Suppose that $N = 8$. Plot S/N as a function of p.

(b) Find U/k_BT vs. N for $S/N = 4$.

Problem 33. Here is another way to look at the signal-to-noise ratio.

(a) Show that the energy of a charged parallel-plate capacitor can be written as $\kappa\epsilon_0 E^2 V/2$, where $V = Sd$ is the volume between the plates. This is a special case of a general relationship that the energy per unit volume associated with an electric field is $\kappa\epsilon_0 E^2/2$.

(b) Use the information about the magnitude of the electric field in the cell membrane from Fig. 9.19 to calculate the total electrostatic energy in the membrane.

(c) Compare the ratio of the total electrostatic energy to k_BT when the air field is 300 V m^{-1}. This overestimates the ratio, because the energy is spread over the entire membrane and is not available to interact in one place.

Problem 34. Obtain Eq. 9.79 from the expression $U = -mB\cos\theta$ that was derived in Problem 8.35, by making a suitable expansion for small angles.

Problem 35. Electric fields in the body caused by exposure to power lines are produced by two mechanisms: direct coupling to the power line electric field, and Faraday induction from the power line magnetic field. Consider a high-voltage power line that produces an electric field of 10 kV m^{-1} and a magnetic field of 50 μT (Barnes 1995). Estimate the electric field induced in the human body by these two mechanisms. Which is larger? Compare the strength of these powerline-induced electric fields to the strength of naturally-occurring electric field produced in the body by the heart (estimate the strength of this endogenous field using the data in Fig. 7.23).

Problem 36. Derive the equations for the electric field shown in Fig. 9.19. Use the following method. Let the potentials be $v_{\text{outside}} = A\cos\theta/r^2 - E_1 r\cos\theta$ and $v_{\text{inside}} = Br\cos\theta$, where A and B are unknown constants. At the cell surface, the following boundary condition applies when the cell membrane is thin and obeys Ohm's law:

$$\sigma_{\text{outside}}\left(\frac{\partial v_{\text{outside}}}{\partial r}\right)\Bigg|_{r=a} = \sigma_{\text{inside}}\left(\frac{\partial v_{\text{inside}}}{\partial r}\right)\Bigg|_{r=a} = (v_{\text{outside}} - v_{\text{inside}})\frac{\sigma_{\text{membrane}}}{b}\Bigg|_{r=a}$$

(a) Verify that the expressions for v_{outside} and v_{inside} obey Laplace's equation and behave properly at $r = 0$ and $r = \infty$.

(b) Use the boundary condition to determine A and B.

(c) Use your expressions for the potential to determine the electric fields given in Fig. 9.19.

References

Abramowitz M, Stegun IA (1972) Handbook of mathematical functions with formulas, graphs and mathematical tables. U. S. Government Printing Office, Washington, DC

Adair RK (1991) Constraints on biological effects of weak extremely-low-frequency electromagnetic fields. Phys Rev A 43:1039–1048

Adair RK (1992) Reply to "Comment on 'Constraints on biological effects of weak extremely-low-frequency electromagnetic fields.'" Phys Rev A 46:2185–2187

Adair RK (1993) Effects of ELF magnetic fields on biological magnetite. Bioelectromagnetics 14:1–4

Adair RK (1994) Constraints of thermal noise on the effects of weak 60-Hz magnetic fields acting on biological magnetite. Proc Natl Acad Sci U S A 91:2925–2929

Adair RK (2000) Static and low-frequency magnetic field effects: health risks and therapies. Rep Prog Phys 63:415–454

Adair RK, Astumian RD, Weaver JC (1998) Detection of weak electric fields by sharks, rays and skates. Chaos 8:576–587

Ashcroft F (2012) The spark of life: electricity in the human body. Norton, New York

Astumian RD, Weaver JC, Adair RK (1995) Rectification and signal averaging of weak electric fields by biological cells. Proc Natl Acad Sci U S A 92:3740–3743

Barnes FS (1995) Typical electric and magnetic field exposures at power-line frequencies and their coupling to biological systems. In: Blank M (ed) Electromagnetic fields: biological interactions

and mechanisms. American Chemical Society, Washington, DC, pp 37–55
Bastian J (1994) Electrosensory organisms. Phys Today 47(2):30–37
Bockris JO'M, Reddy AKN (1970) Modern electrochemistry, vol 1. Plenum, New York
Bren SPA (1995) 60 Hz EMF health effects—a scientific uncertainty. IEEE Eng Med Biol 14:370–374
Carstensen EL (1995) Magnetic fields and cancer. IEEE Eng Med Biol 14:362–369
Chandler WK, Hodgkin AL, Meves H (1965) The effect of changing the internal solution on sodium inactivation and related phenomena in giant axons. J Physiol 180:821–836
Crouzy SC, Sigworth FJ (1993) Fluctuations in ion channel gating currents: analysis of nonstationary shot noise. Biophys J 64:68–76
DeFelice LJ (1981) Introduction to membrane noise. Plenum, New York
Denk W, Webb WW (1989) Thermal-noise-limited transduction observed in mechanosensory receptors of the inner ear. Phys Rev Lett 63(2):207–210
Doyle DA, Cabral JM, Pfuetzner RA, Kuo A, Gulbis JM, Cohen SL, Chait BT, MacKinnon R (1998) The structure of the potassium channel: molecular basis of K^+ conduction and selectivity. Science 280: 69–77
Foster KR (1996) Electromagnetic field effects and mechanisms: in search of an anchor. IEEE Eng Med Biol 15(4):50–56
Foster KR, Moulder JE (2013) Wi-Fi and health: review of current status and research. Health Phys 105(6):561–575
Foster KR, Schwan HP (1996) Dielectric properties of tissues. In: Polk C, Postow E (eds) Handbook of biological effects of electromagnetic fields. CRC, Boca Raton, pp 25–102
Grosberg AY, Nguyen TT, Shklovskii BI (2002) Colloquium: the physics of charge inversion in chemical and biological systems. Rev Mod Phys 74: 329–345
Hafemeister D (1996) Resource letter BELFEF-1: biological effects of low-frequency electromagnetic fields. Am J Phys 64:974–981
Hamill OP, Marty A, Neher E, Sakmann B, Sigworth FJ (1981) Improved patch-clamp techniques for high-resolution current recording from cells and cell-free membrane patches. Pflügers Arch 391:85–100
Hille B (2001) Ion channels of excitable membranes, 3rd ed. Sinauer Associates, Sunderland
Honig B, Nicholls A (1995) Classical electrostatics in biology and chemistry. Science 268:1144–1149
Jiang Y, Le A, Chen J, Ruta V, Cadene M, Chait BT, MacKinnon R (2003) X-ray structure of a voltage-dependent K^+ channel. Nature 423:33–41
Kalmijn AJ (1988) Detection of weak electric fields. In: Aetma J et al. (eds) Sensory biology of auatic animals. Springer, New York, pp 151–186
Keynes RD (1994) The kinetics of voltage-gated ion channels. Q Rev Biophys 27(4):339–434
Khurana VG, Moulder JE, Orton CG (2008) There is currently enough evidence and technology available to warrant taking immediate steps to reduce exposure of consumers to cell-phone-related electromagnetic radiation. Med Phys 35:5203–5206
Kirschvink JL (1992) Comment on "Constraints on biological effects of weak extremely-low-frequency electromagnetic fields." Phys Rev A 46:2178–2184
Kirschvink JL, Kobayashi-Kirschvink A, Woodford BJ (1992a) Magnetite biomineralization in the human brain. Proc Natl Acad Sci U S A 89:7683–7687
Kobayashi AK, Kirschvink JL, Nesson MH (1995) Ferromagnetism and EMFs. Nature 374:123
Lamb H (1932) Hydrodynamics. Cambridge University Press, Cambridge
Leuchtag HR, Swihart JC (1977) Steady-state electrodiffusion. Scaling, exact solutions for ions of one charge, and the phase plane. Biophys J 17:27–46
Lewis CA (1979) Ion-concentration dependence of the reversal potential and the single channel conductance of ion channels at the frog neuromuscular junction. J Physiol 286:417–445
Lu J, Fishman HM (1994) Interaction of apical and basal membrane ion channels underlies electroreception in ampullary epithelia of skates. Biophys J 67:1525–1533
Mauro A (1962) Space charge regions in fixed charge membranes and the associated property of capacitance. Biophys J 2:179–198
Moulder JE, Foster KR (1995) Biological effects of power-frequency fields as they relate to carcinogenesis. Proc Soc Expt Biol Med 209:309–324
Moulder JE, Foster KR (1999) Is there a link between exposure to power-frequency electric fields and cancer? IEEE Eng Med Biol 18(2):109–116
Moulder JE, Foster KR, Erdreich LS, McNamee JP (2005) Mobile phones, mobile phone base stations and cancer: a review. Int J Radiat Biol 81(3):189–203
Moy G, Corry B, Kuyucak S, Chung S-H (2000) Tests of continuum theories as models of ion channels. I. Poisson-Boltzmann theory versus Brownian dynamics. Biophys J 78:2349–2362
National Research Council (1997) Committee on the possible effects of electromagnetic fields on biologic systems. Possible health effects of exposure to residential electric and magnetic fields. National Academy Press, Washington, DC
Neher E, Sakmann B (1976) Single-channel currents recorded from membrane of denervated frog muscle fibers. Nature 260:799–802
Nichols CG, Makhina EN, Pearson WL, Sha Q, Lopatin AN (1996) Inward rectification and implications for cardiac excitability. Circ Res 78:1–7
Pallotta BS, Magleby KL, Barrett JN (1981) Single channel recordings of Ca^{2+}-activated K^+ currents in rat muscle cell culture. Nature 293:471–474
Payandeh J, Scheuer T, Zheng N, Catterall WA (2011) The crystal structure of a voltage-gated sodium channel. Nature 475:353–358
Pickard WF (1988) A model for the acute electrosensitivity of cartilaginous fishes. IEEE Trans Biomed Eng 35(4):243–249
Polk C (1994) Effects of extremely-low-frequency magnetic fields on biological magnetite. Bioelectromagnetics 15:261–270
Polk C (1995) Bioelectromagnetic dosimetry. In: Blank M (ed) Electromagnetic fields: biological interactions and mechanisms. American Chemical Society, Washington, DC, pp 57–78
Polk C (1996) Introduction. In: Polk C, Postow E (eds) Handbook of biological effects of electromagnetic fields. CRC, Boca Raton, pp 1–23
Rohs R, West SM, Sosinsky A, Liu P, Mann RS, Honig B (2009) The role of DNA shape in protein-DNA recognition. Nature 461:1248–1253
Shapiro EM, Borthakur A, Gougoutas A, Reddy R (2002) ^{23}Na MRI accurately measures fixed charge density in articular cartilage. Magn Reson Med 47:284–291
Sheppard AR, Swicord ML, Balzano Q (2008) Quantitative evaluations of mechanisims of radiofrequency interactions with biological molecules and processes. Health Phys 95(4):365–396
Sigworth FJ (1993) Voltage gating of ion channels. Q Rev Biophys 27(1):1–40
Tenforde TS (1995) Spectrum and intensity of environmental electromagnetic fields from natural and man-made sources. In: Blank M (ed) Electromagnetic fields: biological interactions and mechanisms. American Chemical Society, Washington, DC, pp 13–35
Tucker RD, Schmitt OH (1978) Tests for human perception of 60 Hz moderate strength magnetic fields. IEEE Trans Biomed Eng 25:509–518

Uehara M, Sakane KK, Maciel HS, Urruchi WI (2000) Physics and biology: bio-plasma physics. Am J Phys 68:450–455

Vecchia P, Matthes R, Ziegelberger G, Lin J, Saunders R, Swerdlow A (eds) (2009) Exposure to high frequency electromagnetic fields, biological effects and health consequences (100 kHz–300 GHz). ICNRP 16/2009. Oberschleißheim, Germany, International Commssion on Non-Ionizing Radiation Protection

Weaver JC (2000) Electroporation of cells and tissues. IEEE Trans Plasma Sci 28:24–33

Weaver JC, Astumian RD (1990) The response of living cells to very weak electric fields: the thermal noise limit. Science 247:459–462

Weaver JC, Astumian RD (1995) Issues relating to causality of bioelectromagnetic fields. In: Blank M (ed) Electromagnetic fields: biological interactions and mechanisms. American Chemical Society, Washington, DC, pp 79–96

Yi M, Nymeyer H, Zhou H-X (2008) Test of the Gouy-Chapman theory for a charged lipid membrane against explicit-solvent molecular dynamics simulations. Phys Rev Lett 101:038103